

RESEARCH ARTICLE | JANUARY 28 2025

How well do empirical molecular mechanics force fields model the cholesterol condensing effect?

Special Collection: **Molecular Dynamics, Methods and Applications 60 Years after Rahman**

J. Sawdon  ; T. J. Piggot  ; J. W. Essex  

 Check for updates

J. Chem. Phys. 162, 044901 (2025)

<https://doi.org/10.1063/5.0238409>



View
Online



Export
Citation

Articles You May Be Interested In

Effects of cholesterol on the binding of the precursor neurotransmitter tryptophan to zwitterionic membranes

J. Chem. Phys. (October 2018)

Molecular dynamics simulations of cholesterol-rich membranes using a coarse-grained force field for cyclic alkanes

J. Chem. Phys. (December 2015)

Parameters for Martini sterols and hopanoids based on a virtual-site description

J. Chem. Phys. (December 2015)



Nanotechnology & Materials Science



Optics & Photonics



Impedance Analysis



Scanning Probe Microscopy



Sensors



Failure Analysis & Semiconductors



Unlock the Full Spectrum.
From DC to 8.5 GHz.
Your Application. Measured.

[Find out more](#)



How well do empirical molecular mechanics force fields model the cholesterol condensing effect?

Cite as: *J. Chem. Phys.* **162**, 044901 (2025); doi: 10.1063/5.0238409

Submitted: 11 September 2024 • Accepted: 27 December 2024 •

Published Online: 28 January 2025



View Online



Export Citation



CrossMark

J. Sawdon,¹  T. J. Piggot,^{1,2,a}  and J. W. Essex^{1,b} 

AFFILIATIONS

¹ School of Chemistry, University of Southampton, Highfield, Southampton SO17 1BJ, United Kingdom

² Chemical, Biological and Radiological Sciences Division, Defence Science and Technology Laboratory (DSTL), Porton Down, Salisbury, Wiltshire SP4 0JQ, United Kingdom

Note: This paper is part of the JCP Special Topic on Molecular Dynamics, Methods and Applications 60 Years after Rahman.

^at.piggot@soton.ac.uk and ^btj.piggot@dstl.gov.uk

^bAuthor to whom correspondence should be addressed: j.w.essex@soton.ac.uk

ABSTRACT

Membrane properties are determined in part by lipid composition, and cholesterol plays a large role in determining these properties. Cellular membranes show a diverse range of cholesterol compositions, the effects of which include alterations to cellular biomechanics, lipid raft formation, membrane fusion, signaling pathways, metabolism, pharmaceutical therapeutic efficacy, and disease onset. In addition, cholesterol plays an important role in non-cellular membranes, with its concentration in the skin lipid matrix being implicated in several skin diseases. In phospholipid membranes, cholesterol increases the tail ordering of neighboring lipids, decreasing the membrane lateral area and increasing the thickness. This reduction in the lateral area, known as the cholesterol condensing effect, results from cholesterol–lipid mixtures deviating from ideal mixing. Capturing the cholesterol condensing effect is crucial for molecular dynamics simulations as it directly affects the accuracy of predicted membrane properties, which are essential for understanding membrane function. We present a comparative analysis of cholesterol models across several popular force fields: CHARMM36, Slurps, Lipid17, GROMOS 53A6_L, GROMOS-CKP, MARTINI 2, MARTINI 3, and ELBA. The simulations of 1,2-dimyristoyl-sn-glycero-3-phosphocholine (DMPC) and 1,2-dioleoyl-sn-glycero-3-phosphocholine (DOPC) membranes with varying cholesterol concentrations were conducted to calculate the partial-molecular areas of cholesterol and other condensing parameters, which are compared to the experimental data for validation. While all tested force fields predict small negative deviations from ideal mixing in cholesterol–DOPC membranes, only all-atom force fields capture the larger deviations expected in DMPC membranes. United-atom and coarse-grained models under-predict this effect, condensing fewer neighboring lipids by smaller magnitudes, resulting in too small deviations from ideal mixing. These results suggest that all-atom force fields, particularly CHARMM36 or Slurps, should be used for accurate simulations of cholesterol-containing membranes.

© 2025 Author(s). All article content, except where otherwise noted, is licensed under a Creative Commons Attribution (CC BY) license (<https://creativecommons.org/licenses/by/4.0/>). <https://doi.org/10.1063/5.0238409>

I. INTRODUCTION

Lipid membranes are one of the most widespread cellular structures. While lipid membranes have long been understood to perform as selective barriers that surround cells, an array of additional roles and functions of these membranes has been discovered. For example, membranes can act as regulators of protein function, as a way to segregate intra-cellular components, and as signaling platforms.^{1,2} Different membranes, both within and across species, have evolved to perform specific functions determined by the composition and arrangement of their components. For example, animal plasma

membranes have evolved to contain a wide-variety of lipids that include many different types of phospholipids, sphingolipids, and sterols. Different lipid species are commonly distributed unevenly, both between membrane leaflets and laterally within a leaflet.^{3–5} This differential distribution enables correct membrane function, for example; phosphoinositol lipids, minor components of the plasma membrane, are predominantly located within the cytoplasmic leaflet of the membrane to perform their role in intra-cellular signaling.⁵

Within the aforementioned plasma membrane, another lipid component essential for correct membrane function is the sterol

molecule cholesterol. Indeed, it is hard to overstate the importance of cholesterol's role as a lipid, as highlighted by its ubiquity in all animal plasma membranes as well as its common occurrence in many other types of membranes. For example, cholesterol has an important role within the stratum corneum membrane and the barrier function of the skin.⁶ Cholesterol makes up a large component of many of the membranes in which it is found; for the example of plasma membranes, this is roughly 40% of the overall lipid content.⁷ Much research into the effects of cholesterol on membrane properties over the past century has demonstrated that cholesterol increases the ordering of lipid tails and therefore decreases the lateral membrane area while increasing the membrane thickness. This increased ordering is believed to arise from the unique structure of cholesterol (Fig. 1), which allows it to enhance the packing together with the surrounding membrane lipid tails. The extent of the cholesterol-induced change has been shown to be dependent on the types of lipids comprising the membrane, with greater effects arising with increased lipid tail length and saturation.^{8–11} While not the only important physiological function of cholesterol,¹² the cholesterol specific ordering of lipid tails decreases membrane permeability and fluidity, alters the mechanical properties of the membrane, and is believed to be essential for correct membrane lateral heterogeneity.¹³

An important property of cholesterol induced lipid ordering is that the reduction observed in the membrane area due to cholesterol ordering is not linear with respect to increasing cholesterol concentration. This phenomenon was first reported by

Leathes¹⁴ as a tendency for the lateral area of cholesterol containing monolayers to deviate negatively from ideal mixing behavior. This negative deviation from ideal mixing in cholesterol-lipid membranes has since been termed the cholesterol condensing effect and is well studied in phosphatidylcholine (PC) lipid membranes both experimentally^{9,10,15,16} and computationally.^{17–27} Such non-ideal mixing behavior occurs because at low cholesterol concentrations, each cholesterol molecule is able to impose an ordering effect on multiple neighboring lipids, causing a decrease in the lateral area of these lipids and therefore a greater overall decrease in the membrane area than expected. At higher concentrations, cholesterol molecules are more likely to be closer together, resulting in an overlap of the effective condensing area of each cholesterol molecule, in turn reducing the magnitude of the condensing effect per cholesterol molecule. More recently, Edholm and Nagle have reported that cholesterol has a negative partial-molecular area at low concentrations in simulations of 1,2-dipalmitoyl-sn-glycero-3-phosphocholine (DPPC) bilayers,⁸ and experimental studies have reported a negative partial-molecular area of cholesterol in 1,2-dimyristoyl-sn-glycero-3-phosphocholine (DMPC) and DPPC membranes^{9–11} but a positive value for 1,2-dioleoyl-sn-glycero-3-phosphocholine (DOPC) membranes.¹¹ The negative partial-molecular areas of cholesterol, where the addition of extra cholesterol molecules results in a smaller overall membrane area, are at the extreme of such non-ideal mixing behavior and the condensing ability of cholesterol. The differences observed between lipids with two fully saturated (DMPC and DPPC) and two monounsaturated (DOPC) lipid tails, including a lack of observed negative partial-molecular area of cholesterol with DOPC, seemingly arise from a weaker cholesterol condensing ability when combined with more disordered, unsaturated, lipid tails.

Molecular dynamics simulation is a powerful tool for membrane analysis, having been routinely used alongside experimental data to provide molecular level insights into cholesterol containing membrane systems.^{17,18,23,25–35} The accuracy of simulations hinges significantly on the ability of force field parameter sets to replicate molecular behaviors. This accuracy is paramount in capturing interactions between system components. In particular, in cholesterol containing membranes, accurately modeling cholesterol-lipid interactions is essential to correctly model the behavior of cholesterol. However, until recently, very little work has been published examining cholesterol simulation models.³⁶ Currently, there are several force fields available, which may be used to model cholesterol containing membranes, but there is a general lack of information regarding the suitability and accuracy of such force field parameters. Recently, the NMRlipids project has aimed to address this problem through primarily a comparison of simulations containing varying concentrations of PC lipids and cholesterol with experimental data regarding C–H order parameters, lipid diffusion, and x-ray scattering data.³⁶ This work demonstrated that all the force field parameters tested had room for improvement with regards to reproducing these experimental data.

Within this work, we sought to further expand the testing of cholesterol force field parameters. In particular, if a force field is to accurately model cholesterol containing membranes, we believe that accurately reproducing the cholesterol condensing effect and predicting the partial-molecular areas of cholesterol similar to experimental values is essential. The following work, therefore, presents

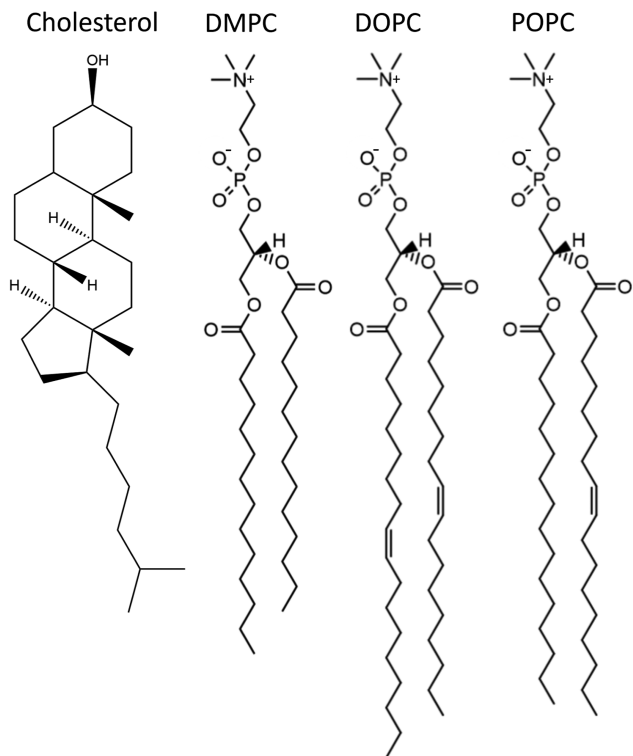


FIG. 1. Molecular structure of cholesterol, DMPC, DOPC, and POPC lipids.

a comprehensive comparison of several force fields and cholesterol models for simulating cholesterol in DMPC and DOPC membranes with the goal of examining the ability of force fields to match the experimental condensation data. In addition, the cholesterol condensing effect in 1-palmitoyl-2-oleoyl-sn-glycero-3-phosphocholine (POPC) membranes is also investigated. The force fields studied are divided into three categories: all-atom force fields (AA), united-atom (UA) force fields, and coarse-grained (CG) force fields. This work, therefore, covers many of the commonly used MD cholesterol force field parameters currently available.

II. MATERIALS AND METHODS

A. Simulation parameters

Force fields included in this analysis are as follows: (i) all-atom force fields: CHARMM36,³⁷ Slurids,³⁸ and Lipid17;^{39–41} (ii) united-atom force fields: GROMOS 53A6_L⁴² (also called GROMOS 54A7) and GROMOS-CKP;⁴³ and (iii) coarse-grained force fields: the MARTINI 2 coarse-grained force field alongside three unique MARTINI cholesterol models, an older model (MARTINI 2.0 cholesterol),⁴⁴ the standard cholesterol model used by MARTINI 2 (MARTINI 2.2 cholesterol),⁴⁵ and a model by Daily *et al.* (MARTINI Daily *et al.*),²¹ the MARTINI 3 force field,^{46,47} and ELBA, a dual-resolution coarse-grained/all-atom force field.⁴⁸ Cholesterol parameters for both of the GROMOS force fields were taken from a manual entry in the Automated Topology Builder (ATB) database.^{49,50} For GROMOS-CKP, the parameters published by Bachar *et al.*⁵¹ were employed for the double bond in oleoyl tails. While our previous work demonstrated that the parameters employed by Kukol⁵² resulted in order parameters around the double bond that were in substantial disagreement with experiment,⁴³ subsequent investigation has identified that Kukol did not correctly employ the parameters published by Bachar *et al.* Tests employing the correct Bachar parameters for the double bond demonstrate minor improvements in the experimental agreement of the order parameters when compared to the original GROMOS-CKP simulations employing standard GROMOS parameters for the double bond.⁵³

Initial all-atom and coarse-grained structures were generated using PACKMOL.⁵⁴ All-atom structures were converted for use in united-atom simulations by removing non-polar hydrogen atoms and for use with the ELBA force field using in-house scripts. To make the conversion from all-atom to united-atom systems as simple as possible for both this work and future studies, all the united-atom lipid and cholesterol GROMACS topology files were modified to rearrange the atom order to match that of the corresponding Chemistry at Harvard Molecular Mechanics (CHARMM) force field topologies. While somewhat laborious, such modifications to the topology files now enable trivial conversion of CHARMM all-atom membrane structures to simulation ready united-atom ones (e.g., through a single grep command) without the need for tools to alter the atom order of the structures.

Each system consisted of 128 total lipids and 4096 water molecules, or the equivalent number of water beads for CG systems. This is a higher level of hydration than conditions employed in the experiments that generated our reference data. However, we note that such a difference in hydration does not impact upon membrane properties or the determined x-ray scattering data.^{55–57}

Membranes consisted of mixtures of either DMPC, POPC, or DOPC and cholesterol across a range of 14 concentrations. Exact lipid compositions are described in the [supplementary material](#). MARTINI systems used the 1,2-dilauroyl-sn-glycero-3-phosphocholine (DLPC) lipid model, which also represents DMPC lipids owing to the lower coarse-grained resolution. The majority of the simulations were performed at lower cholesterol concentrations, where a negative partial-molecular area of cholesterol has been reported and the cholesterol condensing effect is at its strongest.^{8,11} Five repeats were run per cholesterol concentration, each using independent starting structures. All simulations were performed using the 2018 series of the GROMACS simulation package,⁵⁸ except for ELBA, which used the Large-scale Atomic/Molecular Massively Parallel Simulator (LAMMPS) (version 29 Oct 2020).⁵⁹

Systems were minimized using the steepest descent algorithm for 5000 steps, before a three-step equilibration process. During equilibration, a Berendsen thermostat⁶⁰ was used to maintain a temperature of 303.15 K (above the phase transition of all phospholipids tested here), using a coupling constant of 1.0 ps. A semi-isotropic Berendsen barostat⁶⁰ was used to maintain a pressure of 1 bar along the xy plane and z axis (the membrane plane and normal), with a coupling constant of 5.0 ps, and a compressibility of 4.5×10^{-5} bars⁻¹. Lipids and solvent were coupled to separate thermostats. Initially, a NVT equilibration step of 0.25 ns was performed, followed by an NPT equilibration step of 0.125 ns with a time step of 1 fs. The time step was increased to 2 fs for the final equilibration stage of 1 ns.

The ELBA systems utilized a modified NVT equilibration protocol to equilibrate the longer time step. Initial NVT equilibration consisted of a time step of 0.6 fs for 6 ps, followed by increasing the time step to 1.2 and 2.0 fs for 120 and 500 ps. Subsequent equilibration in the NPT ensemble was identical to that used for other systems.

Production simulations were run for 200 ns, using the leapfrog integrator with a 2 fs time step for all-atom systems, a 2 fs time step for united-atom systems, 12 fs for MARTINI 2 systems, 20 fs for MARTINI 3, or a dual time step of 2 and 6 fs for ELBA systems,⁶¹ which employed the reversible reference system propagation algorithm (rRESPA) integrator.⁶² The Nosè–Hoover thermostat⁶³ was used to maintain a temperature of 303.15 K with a time constant of 1.0 ps for all systems except MARTINI, which used the velocity rescale thermostat,⁶⁴ as per published protocols.^{37–43,65} A pressure of 1 bar was maintained using the Parrinello–Rahman barostat,⁶⁶ with a time constant of 5.0 ps for all systems except MARTINI 2 systems, which employed the Berendsen barostat, as per published protocols.^{37–43,65} The particle mesh Ewald (PME) method was used to solve long range electrostatic interactions, except for MARTINI and GROMOS systems, which employed the reaction field method, as used in the original work publishing these force fields. In particular, GROMOS simulations employed a relative dielectric constant beyond the cutoff of 62, as applicable for simple point charge (SPC) water,⁶⁷ while MARTINI simulations employed a relative dielectric constant of 15 within the cutoff and an infinite relative dielectric constant beyond. The linear constraint solver (LINCS) algorithm was used to constrain all bonds involving hydrogen atoms, except for MARTINI systems, where LINCS was used to constrain all bonds. The LINCS order and the number of iterations were set to 4 and 1, respectively, for all simulations except those using the MARTINI 2

TABLE I. Parameters used in simulations.

Force field	LJ type	LJ cutoff (nm)	Electrostatic type	Electrostatic cutoff (nm)
CHARMM36	Force-switch	1.0–1.2	PME	1.2
Slipids	PME	1.0	PME	1.0
Lipid17	Cutoff ^a	1.0	PME	1.0
GROMOS 53A6 _L	Cutoff	1.0	Reaction field	1.0
GROMOS-CKP	Cutoff	1.2	Reaction field	1.2
MARTINI 2 and 3	Potential-shift	1.1	Reaction field	1.1
ELBA	Force-switch	1.0	PME	1.2

^aAn additional dispersion correction was also included.

force field, where the values of 8 and 2 were used due to issues with energy conservation.⁶⁸ The remaining parameters were set to best match those used in the original publications, or parameters commonly used in the literature, and are outlined in Table I. For GROMOS-CKP and GROMOS 53A6_L simulations, the settings employed for the cutoffs were those identified to most accurately reproduce the experimental properties of phospholipid membranes when performing simulations with the Verlet cutoff scheme, as employed in modern versions of the GROMACS software.⁵³

B. Analysis

1. Area per lipid

The average area per lipid, a , was calculated from simulations by dividing the x–y area of the simulation box, A_{x-y} , by the number of lipids per leaflet, N_{leaflet} ,

$$a(x) = \left\langle \frac{A_{x-y}}{N_{\text{leaflet}}} \right\rangle, \quad (1)$$

where $\langle \dots \rangle$ represents the ensemble average and a has been written as a function of the cholesterol mole fraction x , highlighting the effect of cholesterol on the membrane area. All analysis was performed using the last 50 ns of simulations only.

2. Condensation analysis

The partial-molecular area of cholesterol, alongside several other cholesterol condensing parameters, is used for force field validation. These condensing parameters are calculated by fitting a model to the average area per lipid data of membranes across a range of cholesterol concentrations and then calculating the derivatives of the curve for a given cholesterol concentration. Two models are discussed in this work, one using a single non-linear equation and the other using two linear-equations. While all these equations were originally derived by Edholm and Nagle,⁸ in the original publication, only the non-linear equation model was used. The equations defining the models are introduced below.

We can define the average area per lipid of a binary mixture of a PC and a cholesterol lipid as a mole fraction weighted average of the area per lipid of the individual components,

$$a(x) = (1-x)\hat{a}_{pc} + x\hat{a}_{chol}, \quad (2)$$

where x is the cholesterol mole fraction and \hat{a}_{pc} and \hat{a}_{chol} are the constant lipid areas of the PC and cholesterol lipid, respectively. Here

we use “constant” to signify that these values do not change with respect to cholesterol mole fraction. The constant PC lipid area can be calculated from a pure PC lipid membrane, while the constant area of cholesterol is more challenging to define, as cholesterol does not readily form a bilayer. While simple, Eq. (2) is inaccurate in its assertion that PC and cholesterol mixtures result in ideal mixing behavior with respect to lipid areas. To address this approximation, one strategy is to replace the constant area terms with partial-molar area terms, which would be functions of the cholesterol mole fraction. However, as the constant area formulation is enticing from an interpretive perspective, additional terms are instead added to Eq. (2), to capture the cholesterol condensing effect as characterized by a negative deviation from ideal mixing.

For low cholesterol concentrations, each cholesterol added to the membrane will condense the maximum possible number of neighboring lipids, n , resulting in each of the neighboring PC lipids having an area reduced by Δa ,

$$a(x) = (1-x)\hat{a}_{pc} + x(\hat{a}_{chol} - n\Delta a). \quad (3)$$

The deviation from ideal mixing is captured by the remaining parameters, n and Δa , which quantify the reduction in the membrane area per cholesterol molecule as caused by the condensing effect. n is the number of lipids, which are condensed by a single cholesterol molecule, and Δa is the reduction in area associated with the condensing of a single PC lipid. Plotting $\frac{a(x)}{1-x}$ against $\frac{x}{1-x}$ yields a gradient given by $\hat{a}_{chol} - n\Delta a$, providing a graphical method for determining the partial molecular area of cholesterol.^{8,27}

For high cholesterol concentrations, each PC lipid will likely already neighbor a cholesterol molecule, resulting in all PC lipids being condensed, and thus each PC lipid will already have an area reduced by Δa . Adding an additional cholesterol molecule will increase the membrane area by the constant cholesterol area, \hat{a}_{chol} . Thus, in the limit of high cholesterol concentration, the membrane area behavior is governed by the following equation:

$$a(x) = (1-x)(\hat{a}_{pc} - \Delta a) + x\hat{a}_{chol} \quad (4)$$

Least squares regression was used to fit Eqs. (3) and (4) to the area per lipid data. We note that while this model is termed the two linear-equation model, as both equations are fit simultaneously (i.e., as parameters are shared between equations, residuals are calculated across both equations and minimized simultaneously), the model is

in fact non-linear. Standard errors were estimated from the parameter covariance matrix using a linear approximation to the model function around the optimum.⁶⁹

The partial-molecular area of cholesterol $a_{\text{chol}}^{\text{pm}}$ may be calculated as the constant area of cholesterol \hat{a}_{chol} minus how much it condenses the membrane,

$$a_{\text{chol}}^{\text{pm}} = \hat{a}_{\text{chol}} - n\Delta a. \quad (5)$$

This corresponds to the intersect of the low cholesterol region linear equation [Eq. (3)] with the ordinate $x = 1$, which is commonly how partial areas are calculated.^{8,10}

Finally, we note that previously a single non-linear equation was used to model the cholesterol condensing effect across the whole range of cholesterol concentrations, which is also derived by Edholm and Nagle,⁸

$$a(x) = c_0 + c_1x + c_2(1-x)e^{-c_3x}, \quad (6)$$

where

$$c_0 = \hat{a}_{\text{pc}} - \Delta a, \quad (7a)$$

$$c_1 = \Delta a + \hat{a}_{\text{chol}} - \hat{a}_{\text{pc}}, \quad (7b)$$

$$c_2 = \Delta a, \quad (7c)$$

$$c_3 = n. \quad (7d)$$

Further details on this single equation model can be found in Ref. 8.

C. Lipid tail order parameters

The lipid acyl tail order parameters (S_{CH}) were calculated using the following equation:

$$S_{\text{CH}} = |(3 \cos^2 \theta - 1)/2|, \quad (8)$$

where θ is the angle between the CH bond vector and the Z axis of the simulation cell. Order parameters were then averaged over the CH bonds of both lipid tails and all PC lipids in the system. The lipid tail positions corresponding to carbon atoms involving double bonds were excluded as their corresponding order parameter values are very low and therefore skew the comparison of DMPC with POPC and DOPC lipids.

III. RESULTS

The average lipid areas were calculated across a range of cholesterol concentrations for DMPC and DOPC membrane simulations and were used to fit the cholesterol condensing effect models. Initially, the single non-linear equation model [Eq. (6)] was fitted to the data. Two sets of experimental data report the average lipid areas for DMPC and DOPC across a range of cholesterol concentrations: the data of Hung *et al.*⁷⁰ and the data of Pan *et al.*¹¹ Both experimental datasets were acquired from the original publications, using WebPlotDigitizer to extract numerical data from plots.⁷¹ For experimental datasets from Pan *et al.* and Hung *et al.*, and the simulation data presented here, this single non-linear equation resulted in significant fitting issues, as is further discussed in Appendix A. As such,

two linear-equations [Eqs. (3) and (4)], also derived by Edholm and Nagle,⁸ were used to model the area per lipid at limiting low and high cholesterol concentrations.

A. Two linear-equation model

Owing to the poor fitting behavior of the single non-linear equation model (see Appendix A), Eqs. (3) and (4) were fit to the lipid area data at low and high cholesterol concentration regions ($x < 0.2$ and $x > 0.3$). These cutoffs were chosen as they define the linear regions of the linear response of lipid area with respect to increasing membrane cholesterol content. The resulting fits are presented in Figs. 2 and 3 for DMPC and DOPC membranes, respectively. The experimental data from Hung *et al.*⁷⁰ and Pan *et al.*¹¹ are included in the analysis for comparison. However, the data from Pan *et al.* have only four observations, too few to fit this model. Parameters calculated from fitting the two linear-equation model to simulation and Hung *et al.* data are presented in the [supplementary material](#) (Table S1).

Although the data of Pan *et al.* have too few data points to fit the two linear equation model, they have been included to provide a qualitative measure of experimental error. The experimental datasets appear to be more similar in DOPC membranes compared to DMPC membranes. For DMPC membranes, the inter-dataset difference appears to be largest in the cholesterol mole fraction region of 0.2–0.3; however, there are no data from the Pan *et al.* dataset for cholesterol mole fractions above this range. Overall, the comparison between experimental datasets is limited in its ability to assess the experimental error, highlighting the need for more experimental data over a wide range of cholesterol concentrations.

It is clear from the plots (Figs. 2 and 3) and the high R^2 values of the fits (see Tables S3 and S4 of the [supplementary material](#)) that the two linear fits are sufficient to model the lipid area data. As a means of validating the two linear-equation model in light of the poor fitting behavior of the single non-linear equation model, we first analyzed the results of fitting to experimental data from Hung *et al.*⁷⁰ In the case of the Hung *et al.* DMPC membrane data, the two linear fits predict a DMPC lipid area of $0.60 \pm 0.00 \text{ nm}^2$, in excellent agreement with the data point at $x = 0$ and other literature values.¹¹ This indicates that the fit of the condensing effect parameters (\hat{a}_{chol} , Δa , and n) does not constrain the model to poorly predict the first data point.

For DOPC membranes, the two linear fits to the Hung *et al.* data predict a DOPC lipid area of $0.74 \pm 0.00 \text{ nm}^2$, larger than other experimental values reported in the literature. Previously reported values, also at 30 °C, are 0.67 ,⁷² 0.72 ,¹¹ and 0.72 nm^2 ,⁷³ with the latter two values using the same x-ray methodology. It is somewhat concerning that the former, and arguably more reliable, DOPC area (0.67 nm^2) was calculated using a more robust joint x-ray and neutron refinement approach, as compared to relying only on x-ray data in the case of Hung *et al.* Despite this, the Hung *et al.* dataset is the only dataset available with sufficient observations spanning a range of cholesterol concentrations and therefore is the only dataset that may be used as a benchmark for this analysis. Despite this, the lipid area predicted by the two linear fit method is consistent with the position of the first data point (which represents the DOPC area), suggesting that the divergence from other experimental values arises

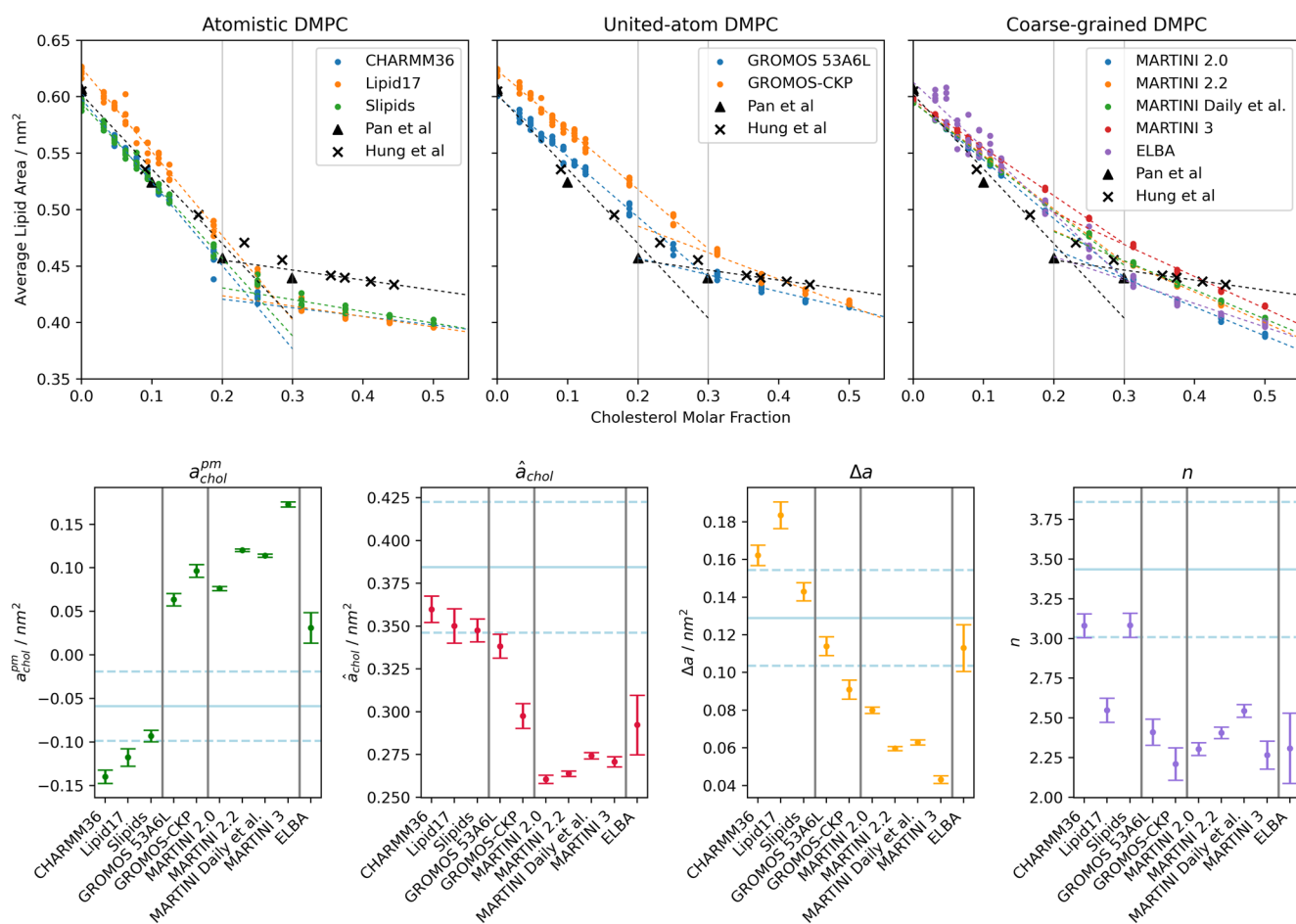


FIG. 2. Top: Average lipid area simulation data of DMPC cholesterol membranes (dots) were used to fit a cholesterol condensing model involving two linear-equations (dashed lines). Experimental data are shown with black crosses and triangles. Only the data of Hung *et al.* are used in the experimental two linear-equation model. Bottom: Calculated cholesterol condensing parameters are also presented. Error bars represent one standard deviation. Fitted parameters from the experimental data of Hung *et al.* are also presented for comparison (blue solid line) (blue dashed line represents one standard deviation).

12 March 2025 11:49:25

from the dataset of Hung *et al.*, and not the two linear-equation model per se.

The two linear fits suggest a partial-molecular area of cholesterol ($a_{\text{chol}}^{\text{pm}}$) of $-0.06 \pm 0.04 \text{ nm}^2$ for the Hung *et al.* DMPC membrane data. For DOPC membranes, $a_{\text{chol}}^{\text{pm}}$ is predicted to be $0.03 \pm 0.04 \text{ nm}^2$, significantly larger than that for DMPC membranes, in qualitative agreement with the literature.¹¹

The predicted constant area of cholesterol (\hat{a}_{chol}) for Hung *et al.* DMPC membranes is $0.38 \pm 0.04 \text{ nm}^2$, falling within the experimental range of $0.3\text{--}0.4 \text{ nm}^2$.^{15,74,75} However, for the DOPC membrane, the model predicts a slightly lower value of $0.35 \pm 0.03 \text{ nm}^2$, despite the expectation of this method for \hat{a}_{chol} to be independent of the degree of the condensing effect. The discrepancy between these values for DMPC and DOPC membranes is small, with each value falling within the standard deviation of the other.

Currently, there are no experimental literature values for the maximum number of lipids a single cholesterol molecule can

condense (n), or by how much the area of a condensed lipid is reduced (Δa). However, the predicted values of 3.4 ± 0.4 and $0.13 \pm 0.03 \text{ nm}^2$ for DMPC membranes and 3.5 ± 0.5 and $0.09 \pm 0.02 \text{ nm}^2$ for DOPC membranes are all physically reasonable. The model predicts that a cholesterol molecule condenses approximately the same number of neighboring lipids for both DMPC and DOPC membranes, with the differences in cholesterol condensation arising from by how much these lipids are condensed.

Overall, the two linear-equation model appears to adequately describe the data from Hung *et al.* and the data from the simulations performed here, of which both show linear behavior in the low and high cholesterol concentration regions.

B. Force field comparison

Having validated the two linear-equation model with the experimental data, the model was fitted to the simulation data. Here, several force fields are tested in their ability to accurately reproduce

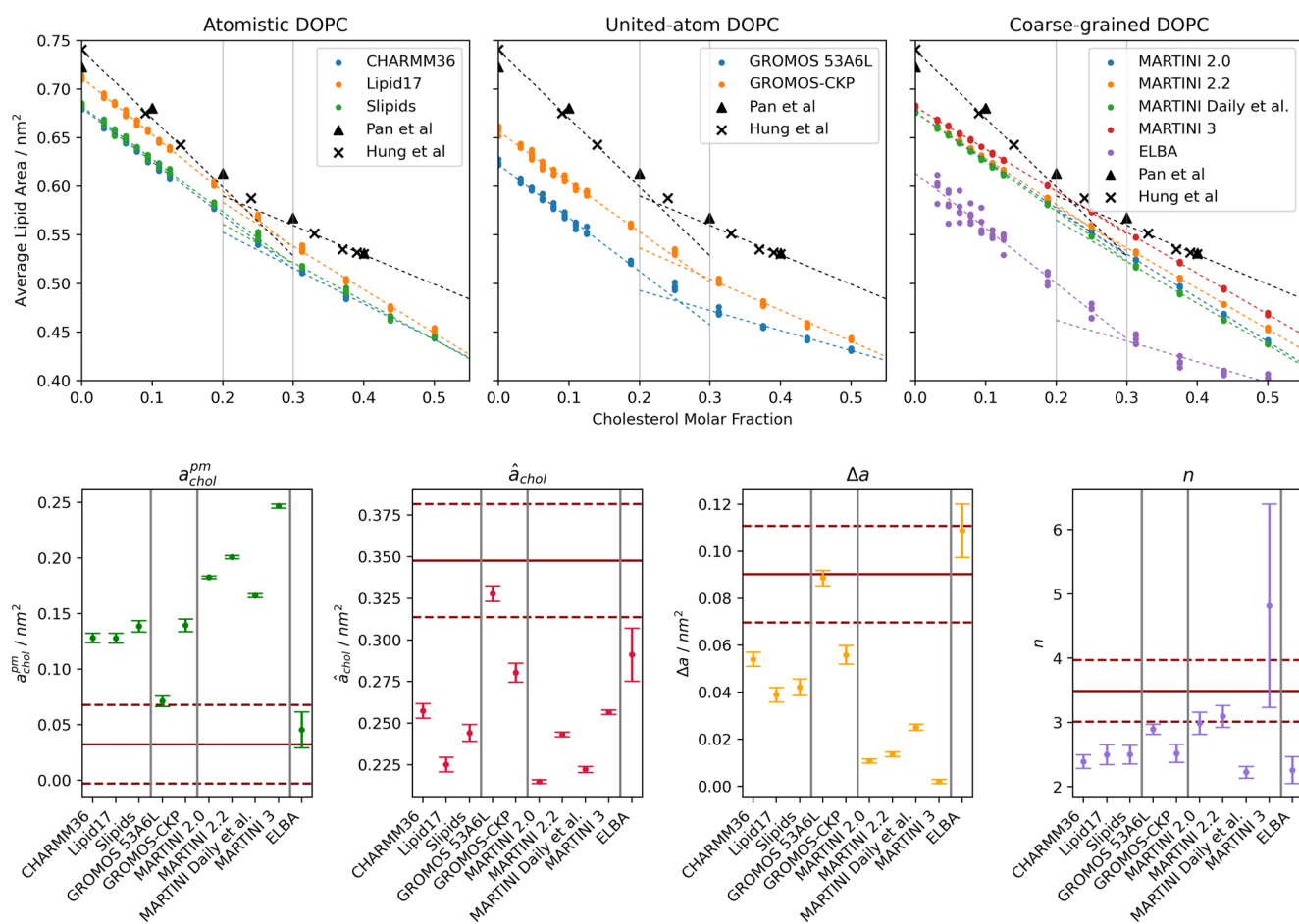


FIG. 3. Top: Average lipid area simulation data of DOPC cholesterol membranes (dots) were used to fit a cholesterol condensing model involving two linear-equations (dashed lines). Experimental data are shown with black crosses and triangles. Only the data of Hung *et al.* are used in the experimental two linear-equation model. Bottom: Calculated cholesterol condensing parameters are also presented. Error bars represent one standard deviation. Fitted parameters from the experimental data of Hung *et al.* are also presented for comparison (red solid line) (red dashed line represents one standard deviation).

12 March 2025 11:49:25

the experimental data, in terms of the cholesterol condensing do effect parameters.

1. All-atom force fields

a. CHARMM36. The CHARMM36 force field predicts an $a_{\text{chol}}^{\text{pm}}$ of $-0.14 \pm 0.01 \text{ nm}^2$ for DMPC membranes, the most negative of all the force fields tested here and, indeed, slightly too negative compared to the fit to the experimental data of Hung *et al.*, which predicts $a_{\text{chol}}^{\text{pm}} = -0.06 \pm 0.04 \text{ nm}^2$.

The other condensing parameters predicted from the two linear-equation model allow further insights into differences between the CHARMM36 force field and the experimental data of Hung *et al.* CHARMM36 predicts a cholesterol area (\hat{a}_{chol}) of $0.36 \pm 0.01 \text{ nm}^2$, close to the experimental fit, which predicts $0.38 \pm 0.04 \text{ nm}^2$. The average change in the area of a lipid associated with condensation (Δa) predicted by CHARMM36 is $0.16 \pm 0.01 \text{ nm}^2$,

which is slightly larger than the experimental fit, $0.13 \pm 0.03 \text{ nm}^2$, but falls within one standard deviation. The final condensing parameter, the maximum number of lipids ordered by a cholesterol molecule (n), is predicted to be 3.1 ± 0.1 , which is slightly smaller than the experimental value of 3.4 ± 0.4 but remains within one standard deviation. Overall, the CHARMM36 force field is in reasonable agreement with experiment, although small deviations from the experimental values in all the condensing parameters result in a larger (albeit still low) experimental deviation in the partial-molecular area of cholesterol.

For DOPC membranes, the value of $a_{\text{chol}}^{\text{pm}}$ predicted by CHARMM36 is $0.13 \pm 0.00 \text{ nm}^2$, which is too large compared to the experimental value of $0.03 \pm 0.04 \text{ nm}^2$. CHARMM36 underestimates all the remaining parameters, predicting values for \hat{a}_{chol} , Δa , and n to be 0.26 ± 0.00 , 0.05 ± 0.00 , and $2.4 \pm 0.1 \text{ nm}^2$, respectively, all falling below the experimental values of 0.35 ± 0.03 ,

0.09 ± 0.02 , and $3.5 \pm 0.5 \text{ nm}^2$. In particular, \hat{a}_{chol} falls below to the experimental range of $0.3\text{--}0.4 \text{ nm}^2$ and is also different from the value predicted for DMPC membranes. The differing values of \hat{a}_{chol} predicted in DMPC vs DOPC membranes are discussed later. Thus, it would appear that too small values of Δa and n are partially compensated by a low value of \hat{a}_{chol} , i.e., smaller values of Δa and n result in larger values of $\hat{a}_{\text{chol}}^{\text{pm}}$, while smaller values of \hat{a}_{chol} result in smaller values of $\hat{a}_{\text{chol}}^{\text{pm}}$. This results in a value of $\hat{a}_{\text{chol}}^{\text{pm}}$ which deviates less from the experimental value than the parameters used for its calculation. Thus, the CHARMM36 force field more accurately reproduces the cholesterol condensing effect in DMPC membranes as compared to DOPC membranes; this is the case for many of the force fields discussed below.

b. Slips. Similar to the CHARMM36 force field, the Slips force field is in good agreement with the DMPC data from Hung *et al.* but performs less well for the DOPC data. For DMPC membranes, Slips predicts a $\hat{a}_{\text{chol}}^{\text{pm}}$ of -0.09 ± 0.01 , more closely matching experiment compared to CHARMM36, and in the best agreement of all the force fields tested here. Slips predicts an \hat{a}_{chol} of $0.35 \pm 0.01 \text{ nm}^2$, a Δa of $0.14 \pm 0.00 \text{ nm}^2$, and an n of 3.1 ± 0.1 , all in good agreement with the Hung *et al.* data and marginally outperforming CHARMM36 for values of Δa and n . Overall, for DMPC membranes, Slips is a slight improvement on CHARMM36, representing the best performing force field studied here in its ability to predict the cholesterol condensing parameters of DMPC membranes.

For DOPC membranes, the Slips force field performs less well compared to DMPC membranes and predicts condensing parameters similar to CHARMM36. Slips predicts $\hat{a}_{\text{chol}}^{\text{pm}} = 0.14 \pm 0.01 \text{ nm}^2$, too large compared to experiment. In addition, Slips predicts $\hat{a}_{\text{chol}} = 0.24 \pm 0.01 \text{ nm}^2$, $\Delta a = 0.04 \pm 0.00 \text{ nm}^2$, and $n = 2.5 \pm 0.1$, all too small compared to experiment. Again, the small values of Δa and n are partially compensated by a small value of \hat{a}_{chol} , but not enough to bring $\hat{a}_{\text{chol}}^{\text{pm}}$ more in line with experiment. For DOPC membranes, the Slips force field results are similar to, but slightly worse than, CHARMM36, with the main sources of error coming from the values of \hat{a}_{chol} and Δa .

c. Lipid17. Upon initial inspection, the Lipid17 force field performs similarly to the CHARMM36 and Slips force fields for DMPC membranes, predicting $\hat{a}_{\text{chol}}^{\text{pm}} = -0.12 \pm 0.01 \text{ nm}^2$, in between values predicted by CHARMM36 and Slips. In addition, Lipid17 predicts $\hat{a}_{\text{chol}} = 0.35 \pm 0.01 \text{ nm}^2$ lying inside the experimental range. However, Lipid17 deviates from experiment for the values of $\Delta a = 0.18 \pm 0.01 \text{ nm}^2$ and $n = 2.5 \pm 0.1$, which are too high and too low, respectively. Deviations in these values are in opposite directions, and thus, they have opposite impacts on $\hat{a}_{\text{chol}}^{\text{pm}}$, which largely cancel. This results in Lipid17, predicting a value of $\hat{a}_{\text{chol}}^{\text{pm}}$ similar to CHARMM36 and Slips despite under-performing in terms of reproducing both Δa and n . This highlights the utility of calculating cholesterol condensing parameters in addition to partial-molecular areas.

For DOPC, Lipid17 predicts condensing parameters very similar to CHARMM36 and Slips, with the only difference being that Lipid17 predicts $\hat{a}_{\text{chol}} = 0.23 \pm 0.00 \text{ nm}^2$, which is too small compared to experiment and slightly smaller than the values from CHARMM36 and Slips.

2. United-atom force fields

a. GROMOS 53A6_L. For DMPC membranes, the GROMOS 53A6_L force field predicts $\hat{a}_{\text{chol}}^{\text{pm}}$ to be $0.06 \pm 0.01 \text{ nm}^2$, which is positive and deviates from the experimental value more than any of the all-atom force fields studied. GROMOS 53A6_L predicts a constant cholesterol area, \hat{a}_{chol} , of $0.34 \pm 0.01 \text{ nm}^2$, in good agreement with the experimental value of 0.38 nm^2 , and also predicts $\Delta a = 0.11 \pm 0.00 \text{ nm}^2$, which is smaller than the experimental value of $0.13 \pm 0.03 \text{ nm}^2$, but within one standard deviation. For n , the GROMOS 53A6_L force field deviates more from experiment, predicting 2.4 ± 0.1 , significantly smaller than the experimental value of 3.4 ± 0.4 .

For DOPC membranes, the GROMOS 53A6_L force field predicts an $\hat{a}_{\text{chol}}^{\text{pm}}$ value of $0.07 \pm 0.00 \text{ nm}^2$, which is too large compared to the experimental value of $0.03 \pm 0.04 \text{ nm}^2$ but is an improvement compared to the all-atom force fields studied here. Furthermore, GROMOS 53A6_L predicts $\hat{a}_{\text{chol}} = 0.33 \pm 0.00 \text{ nm}^2$, which is slightly too small compared to the experimental value of $0.35 \pm 0.03 \text{ nm}^2$. Finally, GROMOS 53A6_L predicts $\Delta a = 0.09 \pm 0.02 \text{ nm}^2$, identical to the experimental value, and $n = 2.9 \pm 0.1$, which is too small compared to experiment. While GROMOS 53A6_L slightly under-predicts the cholesterol condensing effect in DOPC membranes, the remaining condensing parameters are in good experimental agreement. Overall, GROMOS 53A6_L underestimates the magnitude of the cholesterol condensing effect in DMPC membranes but is in relatively good agreement with DOPC membranes, improving on all-atom models in this regard. For both lipid types, the main source of error lies in under-predicting the number of lipids condensed by a single cholesterol molecule.

b. GROMOS-CKP. Despite being in the GROMOS family of force fields, and employing the same cholesterol model, GROMOS-CKP differs from GROMOS 53A6_L in terms of this cholesterol condensing effect analysis. For DMPC membranes, GROMOS-CKP predicts $\hat{a}_{\text{chol}}^{\text{pm}} = 0.10 \pm 0.01 \text{ nm}^2$, $\hat{a}_{\text{chol}} = 0.30 \pm 0.01 \text{ nm}^2$, $\Delta a = 0.09 \pm 0.01 \text{ nm}^2$, and $n = 2.2 \pm 0.1$, all deviating more from the Hung *et al.* values compared to the GROMOS 53A6_L force field. Thus, the GROMOS-CKP force field slightly under-performs the GROMOS 53A6_L for DMPC membranes, with a low predicted value of \hat{a}_{chol} partially compensated by the low predicted values of Δa and n .

For DOPC membranes, the GROMOS-CKP force field predicts $\hat{a}_{\text{chol}}^{\text{pm}}$ to be $0.14 \pm 0.01 \text{ nm}^2$, deviating from the experimental value more than GROMOS 53A6_L. The value of \hat{a}_{chol} predicted by GROMOS-CKP is $0.28 \pm 0.01 \text{ nm}^2$ falling under the experimental range of $0.3\text{--}0.4 \text{ nm}^2$, but similar to the value predicted by GROMOS-CKP in DMPC membranes, in contrast to many of the other force fields studied here. GROMOS-CKP predicts a value of Δa of $0.06 \pm 0.00 \text{ nm}^2$, which is in good agreement with the experimental value, but still deviates more than GROMOS 53A6_L, and also predicts a $n = 2.5 \pm 0.1$, which is significantly lower than the experimental value. Similarly to its performance for DMPC membranes, for DOPC membranes, GROMOS-CKP performs worse than GROMOS 53A6_L, with a small value of \hat{a}_{chol} partially compensating for small Δa and n values. If the force field more accurately predicted the constant area of cholesterol with no other modification, it would overall perform worse in regard to capturing the cholesterol condensing effect.

3. Coarse-grained force fields

a. MARTINI 2. Three cholesterol models were tested with the MARTINI 2 force field: the old MARTINI 2.0 cholesterol model⁴⁴ (denoted MARTINI 2.0), a newer MARTINI 2.2 cholesterol model incorporating virtual sites to add asymmetry to the molecule⁴⁵ (denoted MARTINI 2.2), and a model published by Daily *et al.*²¹ further increasing the asymmetry and resolution of the model by using smaller beads (denoted MARTINI Daily *et al.*). Overall, the MARTINI force field, irrespective of which cholesterol model is used, performs the least well as compared to the other force fields studied here. For both DMPC and DOPC membranes, the MARTINI force field significantly under-predicts the magnitude of the cholesterol condensing effect.

For DMPC membranes, the MARTINI 2.0 force field predicts the lowest value of $a_{\text{chol}}^{\text{pm}}$ of $0.08 \pm 0.00 \text{ nm}^2$, compared to 0.12 ± 0.00 and $0.11 \pm 0.00 \text{ nm}^2$ as predicted by MARTINI 2.2 and MARTINI Daily *et al.*, respectively. Interestingly, all the MARTINI cholesterol models predict similar values of \hat{a}_{chol} , with MARTINI 2.0 and 2.2 predicting a value of $0.26 \pm 0.00 \text{ nm}^2$, while MARTINI Daily *et al.* predicts a value of $0.27 \pm 0.00 \text{ nm}^2$. All these values lie below the experimental range of $0.3\text{--}0.4 \text{ nm}^2$. In addition, the MARTINI models also predict similar values of Δa , with the MARTINI 2.0 model predicting $0.08 \pm 0.00 \text{ nm}^2$, and MARTINI 2.2 and Daily *et al.* both predicting $0.06 \pm 0.00 \text{ nm}^2$, all significantly lower than the experimental value of $0.13 \pm 0.03 \text{ nm}^2$. The models predict slightly different values for n ; MARTINI 2.0 predicts 2.3 ± 0.00 , MARTINI 2.2 predicts 2.4 ± 0.00 , and MARTINI Daily *et al.* predicts 2.5 ± 0.00 . These values of n are similar to values predicted by the united-atom force fields and are too small compared to experiment, 3.4 ± 0.4 . For DMPC membranes, the MARTINI cholesterol models tested here are in overall poor agreement with experiment, all predicting values of $a_{\text{chol}}^{\text{pm}}$ significantly larger than experiment. This is caused by the cholesterol molecules only slightly condensing neighboring lipids as suggested by the low Δa value. In addition, the values of $a_{\text{chol}}^{\text{pm}}$ are artificially low, caused by the cholesterol models being un-physically small compared to experiment.

For DOPC membranes, the MARTINI cholesterol models are again in poor agreement with the Hung data, suffering from the same issues of predicting values of \hat{a}_{chol} , Δa , and n , which are all significantly smaller than the experimental Hung *et al.* data, while predicting values of $a_{\text{chol}}^{\text{pm}}$, which are too large.

Overall, the MARTINI 2 force field and cholesterol models tested here poorly capture the cholesterol condensing effect, predicting values of $a_{\text{chol}}^{\text{pm}}$ too large for both DMPC and DOPC membranes. This deviation from the experimental data would be even greater if the MARTINI cholesterol models had a larger, more accurate area. Small values of Δa and n suggest that the MARTINI cholesterol models have a relatively small impact on neighboring lipids, condensing too few by an amount that is too small.

b. MARTINI 3. The MARTINI 3 force field has undergone significant re-parameterization compared to MARTINI 2. Both PC lipids⁴⁷ and cholesterol⁴⁸ have updated topologies and parameter sets to take advantage of the new bead selection available in MARTINI 3. For DMPC membranes, MARTINI 3 predicts $a_{\text{chol}}^{\text{pm}} = 0.17 \pm 0.00 \text{ nm}$, deviating from experiment more than any of the MARTINI 2 cholesterol systems. MARTINI 3 predicts $\hat{a}_{\text{chol}} = 0.27 \pm 0.00 \text{ nm}^2$, smaller than experiment and similar to values predicted

by MARTINI 2. Interestingly, the MARTINI 3 system predicts Δa to be $0.04 \pm 0.00 \text{ nm}^2$, significantly lower than both experiment and what is predicted by MARTINI 2. Finally, MARTINI 3 predicts n to be 2.3 ± 0.01 , which is too small compared to experiment but similar to values predicted by MARTINI 2.

For DOPC membranes, MARTINI 3 predicts $a_{\text{chol}}^{\text{pm}} = 0.25 \pm 0.00 \text{ nm}^2$, again too large compared to experiment and larger than MARTINI 2 predictions. MARTINI 3 predicts $\hat{a}_{\text{chol}} = 0.26 \pm 0.00 \text{ nm}^2$, which is too small compared to experiment but is larger than predicted by MARTINI 2, and thus an improvement. Interestingly, MARTINI 3 predicts the largest value of n for DOPC membranes (4.8 ± 1.6), which is too large compared to experiment. The relatively high error of n likely comes from the value of $\Delta a = 0.00 \pm 0.00$, allowing increased freedom in n during fitting. Overall, MARTINI 3 appears to model the cholesterol condensation effect less accurately compared to MARTINI 2.

c. ELBA. The ELBA force field is set up in a dual-resolution configuration, using an all-atom model for cholesterol, specifically the CHARMM36 model, and a coarse-grained model for the PC lipid. For DMPC membranes, the ELBA force field predicts an $a_{\text{chol}}^{\text{pm}}$ value of $0.03 \pm 0.02 \text{ nm}^2$, which is too large compared to experiment. Interestingly, ELBA's prediction of $a_{\text{chol}}^{\text{pm}}$ is an improvement on the united-atom GROMOS force fields but not as good as the all-atom force fields. The value of \hat{a}_{chol} predicted by ELBA is $0.29 \pm 0.02 \text{ nm}^2$, marginally outside of the experimental range of $0.3\text{--}0.4 \text{ nm}^2$. ELBA predicts a value of $\Delta a = 0.11 \pm 0.01$, in fair agreement with experiment, and a value of $n = 2.3 \pm 0.2$, which is too small.

It is noteworthy that ELBA uses the CHARMM36 cholesterol model but predicts a different value of \hat{a}_{chol} . From the plot of the fit in Fig. 2, it can be observed that for the ELBA force field, the area per lipid is not linear with respect to the cholesterol mole fraction for mole fractions above 0.3. Owing to this, the two linear-equations were refit using only the data above 0.35, where the three remaining data points exhibit a linear behavior. The resulting fit has no change in $a_{\text{chol}}^{\text{pm}}$ but differs in the remaining parameters [see Table S3 of the [supplementary material](#), denoted as ELBA ($x > 0.35$)]. The new value of \hat{a}_{chol} ($0.32 \pm 0.03 \text{ nm}^2$) has been brought significantly closer to the CHARMM36 value ($0.36 \pm 0.01 \text{ nm}^2$), with the remaining difference possibly caused by differences in the packing behavior of the cholesterol model in the coarse-grained ELBA lipid environment compared to the all-atom CHARMM36 environment. The updated fit predicts $\Delta a = 0.13 \pm 0.02 \text{ nm}^2$, matching the experimental value, but predicts $n = 2.1 \pm 0.2$, significantly lower than experiment. ELBA also introduces scaling factors into the mixing rules for interactions between the all-atom and coarse-grained subsystems, affecting the Lennard-Jones interactions and thus the bead/atom sizes. Overall, for DMPC membranes, the ELBA force field predicts that cholesterol orders too few neighboring lipid molecules.

In the case of DOPC membranes, ELBA predicts $a_{\text{chol}}^{\text{pm}} = 0.05 \pm 0.02 \text{ nm}^2$ and is in the best agreement with the experimental value compared to the other force fields studied here. ELBA predicts $\hat{a}_{\text{chol}} = 0.29 \pm 0.02 \text{ nm}^2$ in DOPC membranes, just under the experimental range of $0.3\text{--}0.4 \text{ nm}^2$, and this time larger than the value predicted by CHARMM36. Finally, ELBA predicts values of $\Delta a = 0.11 \pm 0.01 \text{ nm}^2$ in fair agreement with experiment, but too

large, and $n = 2.3 \pm 0.2$, significantly lower than experiment. For DOPC membranes, ELBA is in fair agreement with the experimental data but predicts the constant cholesterol area and the number of lipids ordered by cholesterol to be too small. Overall, the performance of ELBA in capturing the cholesterol condensing effect is more similar to the united-atom force fields tested here, outperforming MARTINI, but under-performing against the all-atom force fields.

C. POPC cholesterol containing membranes

POPC-cholesterol systems were simulated owing to POPC having a tail saturation character between that of DMPC and DOPC, with the aim that this may offer additional insights into the role of saturation on the cholesterol condensing effect. As there are no experimental data characterizing POPC-cholesterol membrane areas over a range of cholesterol concentrations for validation, only all-atom POPC-cholesterol simulations were performed, owing to these force fields previously performing the most consistently accurate. While GROMOS 53A6_L performs more accurately for DOPC membranes, it fails to predict a negative value of $a_{\text{chol}}^{\text{pm}}$ for DMPC membranes. The two linear-equation model was fitted to the lipid area data, and the results are presented in Fig. 4 and Table S5 of the [supplementary material](#). For each force field, the corresponding

parameters from fits to DMPC and DOPC membranes are included for comparison.

The condensing parameters for POPC membranes overall suggest that the cholesterol condensing effect behavior in POPC membranes lies somewhere in between that of DMPC and DOPC membranes. All three of the all-atom force fields predict positive values of $a_{\text{chol}}^{\text{pm}}$ close to 0, which are slightly more similar to values reported for DOPC membranes. The remaining parameters all show a similar behavior, falling in between values obtained from the corresponding DMPC and DOPC fits, with a skew toward the DOPC data. The exception is that Lipid17 and Slipids predict the values of n for POPC membranes, which are lower than the DOPC values.

The comparison of parameters between membrane types, in Fig. 4, also highlights the differences in \hat{a}_{chol} . The fitted model aims for \hat{a}_{chol} to be constant and independent of the membrane composition. While the fits to the experimental data of Hung *et al.* yield similar values of \hat{a}_{chol} in DMPC and DOPC membranes, this is clearly not the case for the simulation data.

D. Constrained \hat{a}_{chol} model

During the fitting of the two linear-equations to DMPC and DOPC data, it was observed that the area of cholesterol (\hat{a}_{chol}) differed between the different membranes. In theory, this should not be

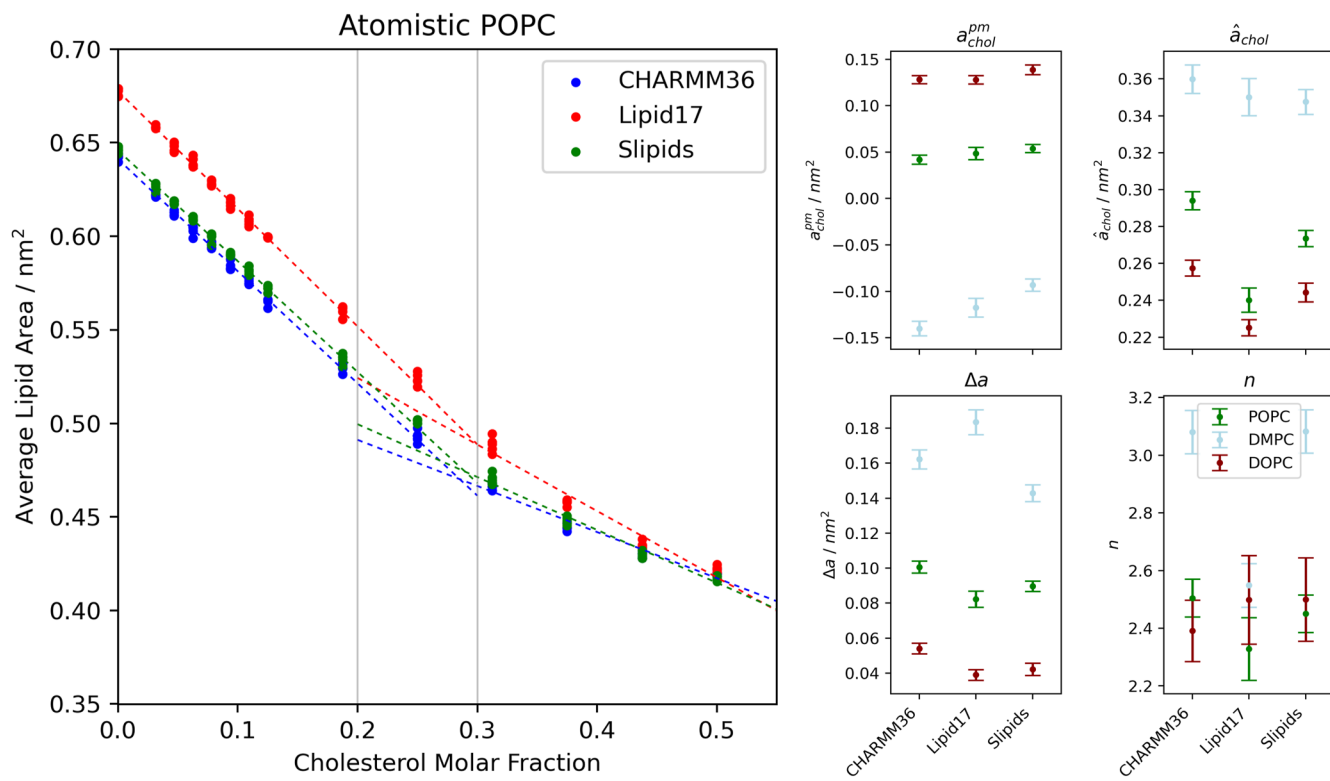


FIG. 4. Left: Average lipid area simulation data of POPC cholesterol membranes (dots) were used to fit a cholesterol condensing model involving two linear fits (dashed lines). Right: Calculated cholesterol condensing parameters are also presented. Data points for the corresponding parameters of DMPC (light blue) and DOPC (dark red) membranes are included for comparison. Error bars show one standard deviation.

the case, with n and Δa varying to accommodate for differences in cholesterol condensing behavior between lipid types. The two linear fits consistently predict smaller values of \hat{a}_{chol} in DOPC membranes compared to DMPC membranes, with the DOPC values regularly falling under the experimental range 0.3–0.4 nm². In an attempt to reconcile these differences, the two linear-equation model was refit to the DOPC data, while constraining \hat{a}_{chol} to the value predicted from the DMPC membrane. The constrained \hat{a}_{chol} fits are presented in Fig. 5, and the fit parameters are listed in Table S6 of the [supplementary material](#).

For the all-atom force fields, the fits to the low cholesterol region remain largely unaltered, aligning well with the data. Conversely, for the high cholesterol concentration region, the constrained fits are less well aligned with the underlying lipid area data, with the model predicting a too shallow gradient than suggested by the data, as can be observed in Fig. 5 (top) and from the increase in mean absolute error (MAE) associated with the constrained fit

(see Table S6 of the [supplementary material](#)). Interestingly, for the united-atom, and coarse-grained force fields, this issue is less pronounced, with a reasonable agreement with the underlying data points across the full range.

We note that the constraining values of \hat{a}_{chol} have little impact on the resulting values of $a_{\text{chol}}^{\text{pm}}$, with the other condensing parameters shifting to offset the imposed change in \hat{a}_{chol} . The changes in condensing parameters are most pronounced for the all-atom force fields, which result in increased values of Δa but decreased values of n . As the decrease in n is of a larger magnitude compared to Δa , this also compensates for the increase in \hat{a}_{chol} , rationalizing the consistency of $a_{\text{chol}}^{\text{pm}}$ values between constrained and unconstrained fits.

These results suggest that the predicted values of $a_{\text{chol}}^{\text{pm}}$ are relatively insensitive to the exact value of \hat{a}_{chol} , with the other cholesterol condensing parameters adjusting to compensate. The low sensitivity to the underlying parameters is favorable behavior and allows

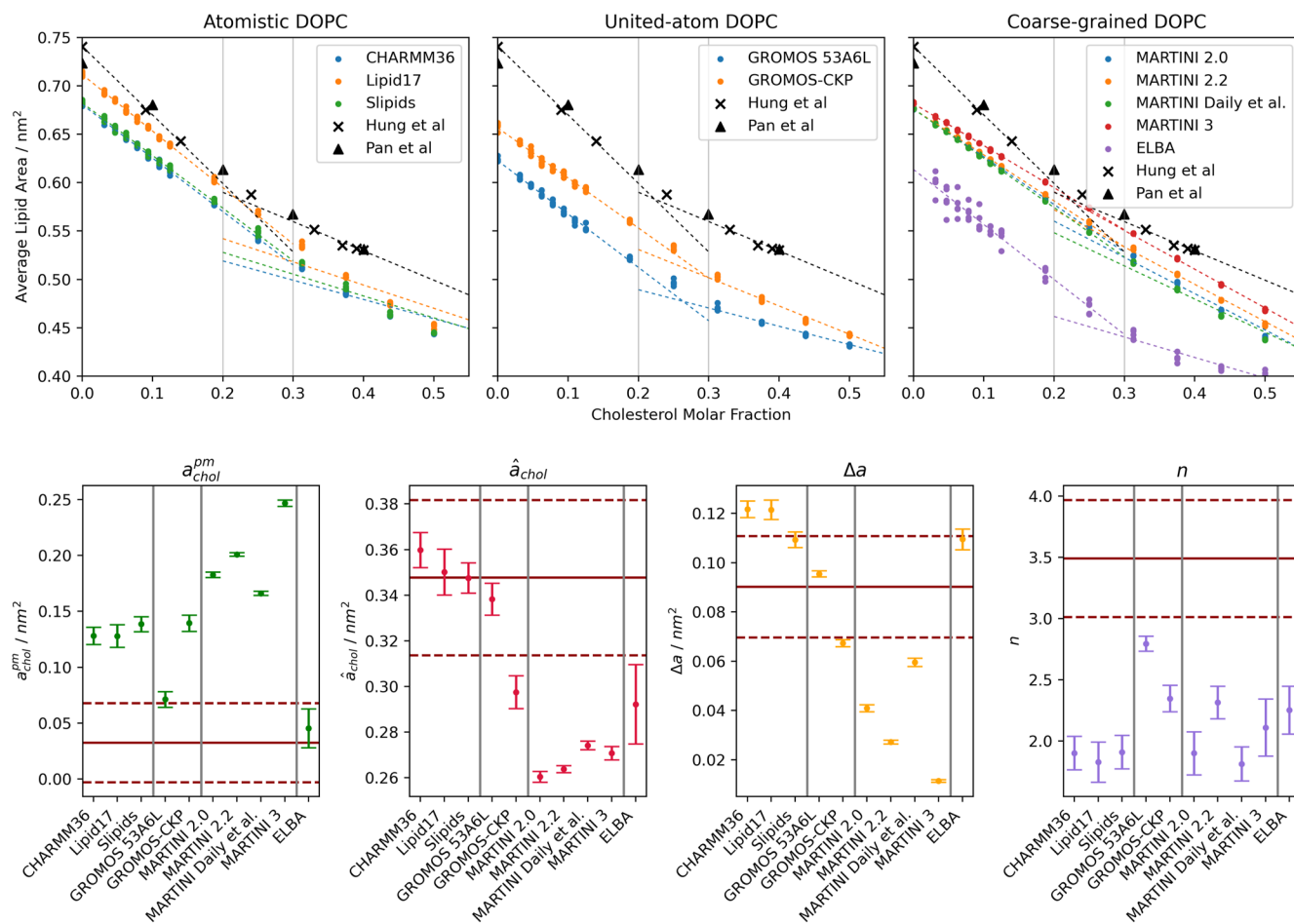


FIG. 5. Constrained \hat{a}_{chol} results. Top: Average lipid area simulation data of DOPC cholesterol membranes (dots) were used to fit a cholesterol condensing model involving two linear fits (dashed lines). Bottom: Calculated cholesterol condensing parameters are also presented. The experimental data of Hung *et al.* are also presented for comparison (red solid line) (red dashed line represents one standard deviation of the value obtained by fitting to the experimental data). Error bars represent one standard deviation.

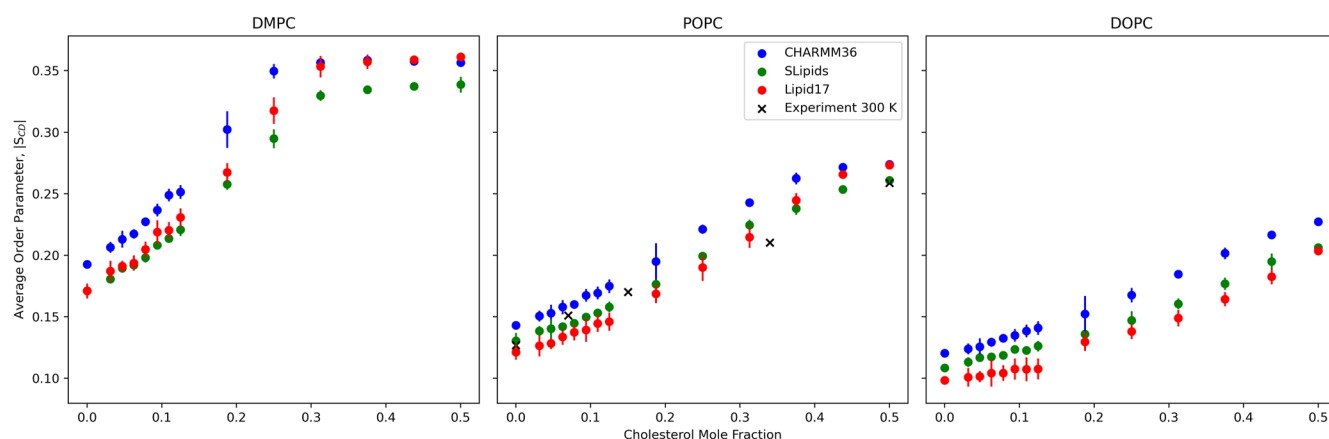


FIG. 6. Average lipid tail order parameters of all-atom simulations of cholesterol containing membranes. The average was taken over each carbon in each acyl tail. Experimental data for the POPC-cholesterol systems from Ref. 77 are depicted with cross marks. Tail positions corresponding to double bonded carbon atoms were excluded from averaging.

for increased confidence in the predicted values of $a_{\text{chol}}^{\text{pm}}$ as the differences in the underlying parameters only have a small impact.

E. Average lipid tail order parameters

Increased lipid tail order is believed to be central to the mechanism of cholesterol condensation, in which each cholesterol imposes order on neighboring PC lipids.⁷⁶ To further investigate the cholesterol condensing effect in PC membranes, lipid acyl tail order parameters were calculated and averaged over each carbon and each tail for a given cholesterol concentration and are presented in Fig. 6. The experimental POPC order parameters from Ref. 77 (extracted from the paper using WebPlotDigitizer⁷¹) are also included in Fig. 6. This analysis was only performed for all-atom simulations, which best reproduce the experimental data and contain hydrogen positions required for order parameter calculation.

For DMPC, POPC, and DOPC membranes, there is a positive correlation between the average lipid tail order parameter and cholesterol concentration. This agrees with the theory that cholesterol molecules impose order on neighboring PC lipid molecules. Interestingly, there is a clear difference in the lipid tail order parameter behavior of each lipid.

In the case of DMPC membranes, there is a steep increase in the averaged order parameter from $x = 0$ to $x = 0.3$, at which point, the values plateau to a value of ~ 0.35 . For DOPC membranes, a much shallower increase is observed across the whole range of cholesterol concentrations tested, with no notable plateau.

POPC membranes have an average lipid tail order parameter character somewhat in between that of DMPC and DOPC. A steady increase is observed across the majority of the cholesterol concentration range until $x = 0.45$, at which point, a plateau begins to be observed, with the average order parameters reaching a final value of ~ 0.275 , in between values observed at similar cholesterol concentrations for DMPC and DOPC membranes. The simulation averaged order parameters are in good experimental agreement across the cholesterol range tested, with the largest discrepancy occurring at a

cholesterol mole fraction of ~ 0.35 . Among the force fields included in this analysis, SLipids shows the best agreement with the experimental results. For a more detailed comparison of simulation and experimental POPC cholesterol order parameters, see Ref. 36.

IV. DISCUSSION

Several lipid force fields have been assessed in their ability to capture the cholesterol condensing effect in terms of recreating experimental cholesterol condensing parameters, including the partial-molecular area of cholesterol. A two linear-equation model used here differs from a previously used model involving a single non-linear equation, despite all equations being derived in the same publication.⁸ The use of the two linear-equation model was necessitated in this work due to the poor fitting behavior of the single non-linear equation model. Although the two linear-equation model offers significantly improved fitting behavior, it is limited by its calculation of only two gradients, which only predict two partial-molecular areas of cholesterol: one at high and the other at low cholesterol concentrations. Despite this, the two linear-equation model is sufficient to model these regions, in which the average area per lipid shows a linear response to increasing cholesterol content. Furthermore, fitting the two linear-equation model to the experimental data of Hung *et al.* results in parameters that are physically plausible. We note that a limitation of the analysis employed here is the lack of robust experimental data over a range of cholesterol concentrations. While the data used are from x-ray experiments, they diverge from observations using more robust joint x-ray and neutron refinement schemes.⁷² Furthermore, more observations over the entire cholesterol range of interest here would allow for better refinement of low and high limiting cholesterol behavior. A comparison of the fitted parameters of cholesterol condensing models allows the analysis to include all data points from both simulation and experimental datasets, but the reliance on experimental lipid areas derived from x-ray experiments comes with a set of assumptions.^{72,78} To address this concern, we also provide a direct

comparison between simulation and experimental x-ray form factors¹¹ in Appendix B. Overall, the form factor analysis we perform offers more mixed results compared to the area analysis. We believe that this may be caused, in part, by the small amount of experimental form factor data available, at only two data points each for DMPC and DOPC lipids. This point is discussed further in Appendix B, again highlighting the need for more experimental data.

An issue observed with the two linear-equation model was that it would produce different values of the constant area per cholesterol (a_{chol}) parameter for different membranes. The model was derived with the aim that a_{chol} should remain constant, with the other model parameters adjusting to account for differences in the cholesterol condensing effect for different membranes. Despite this, constraining the values of a_{chol} has little effect on the predicted values of the partial-molecular area of cholesterol, allowing for greater confidence in these values. Lipid acyl tail order parameters may offer additional insights into this issue. As reported here, the increase in order parameters with increasing cholesterol concentration is dependent upon the saturation character of the lipid tails, and thus, cholesterol imposes order on DMPC, POPC, and DOPC lipids to different extents. In particular, while order parameters plateau at approximately $x = 0.35$ for DMPC membranes, this plateau is observed at $x = 0.45$ for POPC and not at all for DOPC membranes. As such, while the assumption that additional cholesterol condensation is absent at high cholesterol concentrations is true for DMPC, order parameters suggest that this is not the case for DOPC membranes. Thus, the cutoff values for low and high cholesterol regions may need refining for different lipid types. While this study focused on simulations within the low cholesterol concentration region, further data are required in the high and middle cholesterol concentration regions to better characterize the cholesterol condensing effect and further refine the two linear-equation model. While lipid tail order parameters are an alluring target for force field validation, there is an unfortunate lack of experimental data across a range of cholesterol concentrations, as required for such work.

The ELBA force field may offer a unique insight into how force fields capture the cholesterol condensing effect. Despite being a coarse-grained force field, ELBA boasts a significant improvement in accuracy compared to the MARTINI force field with respect to reproducing experimental cholesterol condensing parameters. Indeed, there are several fundamental differences in the philosophy of these force fields, which may lead to such differences: (i) ELBA has a lower degree of coarse-graining compared to MARTINI, especially in the water mapping, (ii) ELBA systems are dual resolution, with the PC lipids modeled at the coarse-grained level and cholesterol modeled at the all-atom level, and (iii) ELBA implements a more realistic electrostatic model compared to MARTINI. It is hard to evaluate which of these properties contribute the most to the improvements associated with ELBA. However, the increased resolution of the all-atom cholesterol molecule will facilitate the asymmetry of the cholesterol model, which is thought to be crucial to the cholesterol condensing effect.⁷⁶

Interestingly, GROMOS 53A6_L and GROMOS-CKP yield different cholesterol condensing parameters, despite employing the same cholesterol model. This highlights that lipid parameters

also play a crucial role in condensation. We propose that the difference in condensing behavior between the two force fields is likely due to the larger radius of the carbonyl carbon atom type (CH0) in GROMOS-CKP compared to that in GROMOS 53A6_L (C).

Furthermore, differences between MARTINI 2 and 3 may offer additional insights into the ability of a force field to capture the cholesterol condensing effect. The MARTINI 3 cholesterol model increases asymmetry by the incorporation of the new *tiny* bead to model two methyl groups of the rough face of cholesterol, in addition to more accurately capturing cholesterol-lipid interactions, as shown by recreating all-atom two-dimensional radial distribution functions of lipids surrounding cholesterol molecules.⁴⁶ Interestingly, despite these improvements, the analysis presented here suggests that MARTINI 3 captures the cholesterol condensing effect less accurately compared to MARTINI 2. Thus, it would appear that improved recreation of the surrounding PC lipid distribution and increasing cholesterol asymmetry are not universal targets for improving cholesterol models. Despite this, we note that molecule topologies and parameters are complex and there is likely a large interplay of parameters driving this phenomenon, which may not be easily assessed independently. Further analysis of MARTINI 2 and MARTINI 3 systems may allow for the determination of molecular features, which bring about cholesterol condensation.

Overall, the analysis presented here suggests that the force field type (all-atom vs united-atom vs coarse-grained) is a reasonable predictor of the accuracy with which the cholesterol condensing effect is captured. We report that all-atom force fields most consistently capture the cholesterol condensing effect when considering both DMPC and DOPC membranes; however, the GROMOS 53A6_L force field is most accurate for DOPC membranes at the expense of poor accuracy for DMPC membranes. Comparatively, the coarse-grained force fields capture the condensing effect less well. It has been previously suggested that the asymmetry between the two faces of cholesterol, specifically the methyl groups protruding from the planar sterol region, plays an important role in the cholesterol condensing effect.⁷⁶ As such, the increased resolution of the methyl groups in the all-atom force fields may play an important role in capturing the cholesterol condensing effect. Despite this, the increase in asymmetry and resolution associated with the Daily *et al.* MARTINI cholesterol model compared to the other MARTINI 2 models tested, offers no significant increase in the force field's accuracy, and indeed, although MARTINI 3 has a more asymmetric cholesterol model, it performed less well in this analysis compared to MARTINI 2. Finally, the data presented here suggest that the CHARMM36 and Slipids force fields best capture the cholesterol condensing effect in DMPC membranes, with Slipids capturing the cholesterol condensing effect in DOPC membranes with slightly better accuracy at the expense of a slightly worse accuracy in DOPC membranes, compared to CHARMM36. For DOPC membranes, our results show that the GROMOS 53A6_L force field is in best agreement with experiment.

V. CONCLUSION

To conclude, we have studied the ability of several commonly used lipid force fields to accurately reproduce the cholesterol

condensing effect. Our results highlight the utility in calculating cholesterol condensing parameters for a more rigorous analysis compared to only reporting partial-molecular cholesterol areas and reveal that the all-atom force fields studied here best capture cholesterol condensation in DMPC membranes. In particular, the CHARMM36 or Slipids force fields are recommended for DMPC membranes, while GROMOS 53A6_L is recommended for DOPC membranes, owing to their accuracy in reproducing cholesterol partial-molecular areas and cholesterol condensing parameters. While the analysis presented here considers simple model membranes, the cholesterol condensing effect holds crucial implications for larger, biologically relevant systems. For example, as lipid raft formation is thought to stem from the cholesterol condensing effect,⁷⁹ simulations studying lipid rafts should use force fields that properly capture this effect. Furthermore, as the cholesterol condensing effect alters membrane thickness, we highlight that careful consideration should be placed on force field choice when modeling membrane bound proteins. These proteins frequently feature hydrophobic transmembrane segments that align with membrane thickness, which may result in membrane deformation or protein tilt when this is not the case.

We have also presented averaged lipid tail order parameters, which suggest a distinct cholesterol condensation profile for DMPC, POPC, and DOPC lipids, which is driven by cholesterol imposing different amounts of order on the same number of lipids. Averaged lipid order parameters also reveal that there is significant cholesterol condensation still occurring at high cholesterol concentrations for POPC and especially for DOPC membranes. Although this brings into question the underlying assumption of the two linear-equation model, that for high cholesterol concentrations, the membrane is fully condensed and no further cholesterol condensation is observed, constraining fitting parameters suggest that the exact values of the cholesterol condensing parameters reported here have little impact on the reported values of the partial-molecular areas of cholesterol.

Further work is required to better characterize the cholesterol condensation effect at higher cholesterol concentrations and in other lipid membranes. Additional experimental data would be invaluable in such further analysis. Such work will be useful to further refine and build upon the cholesterol condensation models and allow for more accurate determination of cholesterol condensing parameters, which offer increased insights into the cholesterol condensing effect compared to solely partial-molecular areas. The analysis performed here would be particularly useful in the development and optimization of cholesterol force fields, ensuring their accuracy in simulating biologically relevant membrane behavior.

SUPPLEMENTARY MATERIAL

The membrane lipid content as well as fitted parameters are provided in the [supplementary material](#).

ACKNOWLEDGMENTS

The authors acknowledge the use of the Iridis 5 high-performance computing facility at the University of Southampton, as well as the resources provided by the Hartree Centre (JADE2)

and HECBioSim (Grant Nos. EP/R029407/1 and EP/X035603/1) for the computational support that facilitated part of this study. This research was funded by the Engineering and Physical Sciences Research Council (EPSRC) and the Defence Science and Technology Laboratory (dstl). We thank Sophia Wheeler for her valuable contribution through her preliminary analysis.

AUTHOR DECLARATIONS

Conflict of Interest

This research was funded by dstl.

Author Contributions

J. Sawdon: Data curation (lead); Formal analysis (lead); Investigation (lead); Methodology (lead); Software (lead); Validation (lead); Visualization (lead); Writing – original draft (lead). **T. J. Piggot:** Data curation (supporting); Funding acquisition (equal); Supervision (supporting); Validation (supporting); Writing – original draft (supporting); Writing – review & editing (supporting). **J. W. Essex:** Conceptualization (lead); Funding acquisition (equal); Project administration (lead); Supervision (lead); Writing – review & editing (lead).

DATA AVAILABILITY

The data that support the findings of this study are openly available at <http://doi.org/10.5281/zenodo.13384821>.

APPENDIX A: SINGLE NON-LINEAR EQUATION MODEL

Initially, the partial-molecular areas of cholesterol, in addition to the cholesterol condensing parameters, were calculated by fitting a single non-linear equation [Eq. (6)]⁸ to the area per lipid data across the whole range of cholesterol concentrations. The non-linear equation model was only fitted to the all-atom data, owing to fitting issues as discussed below. The resulting fits are presented in Fig. 7, and the corresponding parameter values are listed in Table S2 of the [supplementary material](#). In addition to the simulation data presented here and the experimental data of Hung *et al.*, an additional experimental dataset from Pan *et al.*¹¹ is included.

It is clear from the graphical plots that the fit to the experimental data from Pan *et al.* is problematic, as observed by the prediction that the lipid area increases for cholesterol mole fractions above 0.3. For the Pan *et al.* data, the poor model behavior is likely as a result of the dataset having only four data points, equal to the number of parameters. We note that Pan *et al.* also fitted the single non-linear equation to their data in the original publication¹¹ but do not report the cholesterol condensation parameters. Pan *et al.* do report a graphical fit of the single non-linear equation, with no increase in lipid area for high cholesterol mole fractions, as opposed to the results presented here. A possible source of error in our work may be in obtaining the numerical data of Pan *et al.* from a plot in the original publication.¹¹ However, we believe that the uncertainty added by this is less than 1%, as determined by the comparison of the cholesterol mole fraction values obtained from WebPlotDigitizer and the cholesterol mole fractions used by Pan *et al.*¹¹ Owing to this, such

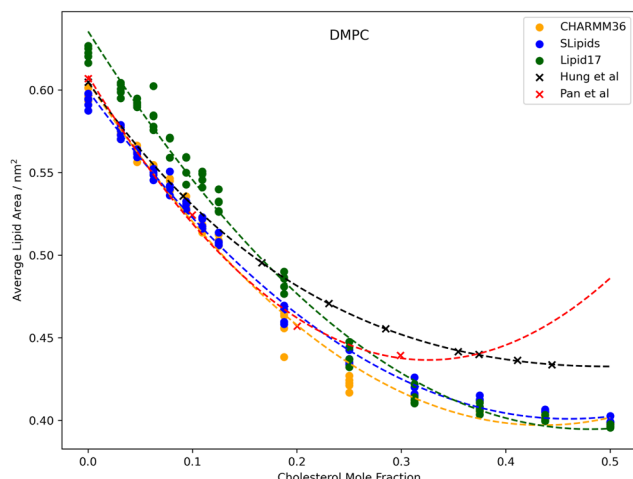


FIG. 7. Average lipid areas of all-atom force field simulations of DMPC cholesterol bilayers across a range of cholesterol concentrations (dots) were used to fit a non-linear cholesterol condensation model (dotted lines). Experimental data from Hung *et al.* and Pan *et al.* (cross marks) were also used to fit the model for comparison.

inaccuracies in extracting the data are unlikely to primarily be the cause of such large optimal parameter values. Finally, the lack of regularization used during fitting here also likely emphasizes the over-fitting, allowing the parameter norm to increase without any penalty. While regularization is often employed in model fitting, the parameters used here have physical implications, and as such, regularization may be used to arbitrarily improve agreement with the experimental data, depending on the magnitude of the penalty applied and the choice of initial parameter values.

While the remaining fits appear to be adequate from the graphical plots, there are clear fitting issues upon inspection of the fitted cholesterol condensing parameter values. Since the parameters in the models used here hold physical significance, it is not sufficient for the model to simply achieve a low error in describing the data. The values of these physical parameters must also align closely with the experimental results or, in cases where ground truth data are unavailable, at least remain physically plausible.

For the simulation data, the non-linear model suggests too large values of Δa , larger than the area of a single PC lipid, and very small values of n . As Δa represents the decrease in lipid area due to condensing, it is physically impossible for this value to exceed the area of a single PC lipid; such a result implies that the area of a condensed lipid is negative. This is particularly true when fit to the Lipid17 data. While the cholesterol condensing parameters appear to be more realistic for the experimental data of Hung *et al.*, the model still predicts that each DMPC lipid is condensed by more than half of its area and that only 2.3 neighboring DMPC lipids are condensed, which is small considering the number of lipids that may pack around a cholesterol molecule. We suggest that the upper limit of Δa should be no more than the difference between the lipid areas of gel phase and liquid phase membranes. For example, DMPC has a gel phase lipid area of 0.47 nm^2 ⁸⁰ but has an area of 0.6 nm^2 above the phase transition. Using this constraint, the upper limit of Δa for a DMPC–cholesterol bilayer is 0.13 nm^2 , in good agreement with

the value predicted by the two linear-equation model when fit to the Hung *et al.* dataset (Table S3). Owing to these fitting issues, it was decided to adopt the two linear-equation model.

APPENDIX B: X-RAY FORM FACTORS

X-ray form factors were calculated from simulations and allow for a more direct comparison between simulation and experiment compared to the comparison of lipid areas, which are calculated from x-ray form factors using a set of assumptions.^{72,78} We note that x-ray form factors calculated directly from simulations have system size effects, which results in issues when defining evaluation metrics, as discussed in Ref. 81. A metric previously defined by the NMR-lipids project⁸¹ has been employed here and involves a comparison of the first form factor minimum of experimental and simulation systems. As this method results in excluding the majority of the data by focusing on a single value of the form factor curve, we have relied more upon the comparison of lipid areas, despite this method having its own limitations.

In-house code was used to calculate x-ray form factors from simulations. While existing code exists, such as SIMtoEXP⁸² and as a part of the NMRlipids data bank project,⁸¹ such implementations impose limitations. SIMtoEXP employs a graphical user interface (GUI), which limits automation, while the NMRlipids data bank approach must be used in conjunction with an NMRlipids data bank, imposing additional steps. The approach used here is implemented in Python and can be used either as a command line tool or as a Python package, allowing for flexible usage for either single simulation trajectory analysis or high throughput analysis. Our code is available at https://github.com/sawds/FF_MAn.

The x-ray form factors are calculated using the standard equation for lipid bilayers without assuming bilayer symmetry,⁸¹

$$F(q) = \left| \int_{-D/2}^{D/2} \Delta\rho_e(z) \exp izq_z dz \right|, \quad (B1)$$

where $\Delta\rho_e(z)$ is the difference in total and bulk solvent electron densities, z is the coordinate along the bilayer normal (assumed to be the simulation z axis), and the integral is over the simulation box of size D , centered at 0. In practice, the integral is replaced with a summation over discrete bins along the simulation z -axis (bilayer normal), with a bin width of 0.2 \AA (matching the bin width used by SIMtoEXP⁸²). The solvent electron density is calculated from the solvent layers above and below the bilayer. Simulation trajectories were centered on PC lipid tail termini CH_3 groups before the form factors were calculated. To calculate the electron density for the united-atom systems, the electron count of non-polar hydrogen atoms, which are not explicitly modeled, are added to the electron count of the bonded heavy atom. Coarse-grained force fields are excluded from this analysis owing to the ambiguity of electron counts of the coarse-grained beads. For example, MARTINI uses the same coarse grained topology to model DMPC and DLPC lipids, despite DLPC having two fewer carbons per acyl tail. Thus, it is not obvious if the CG beads, which remain identical for both lipids, should be assigned different electron counts. Furthermore, some atoms are not assigned to a single bead in MARTINI, again complicating electron assignment. While such hurdles can be overcome, they likely require an in-depth study to quantify the sensitivity of different electron

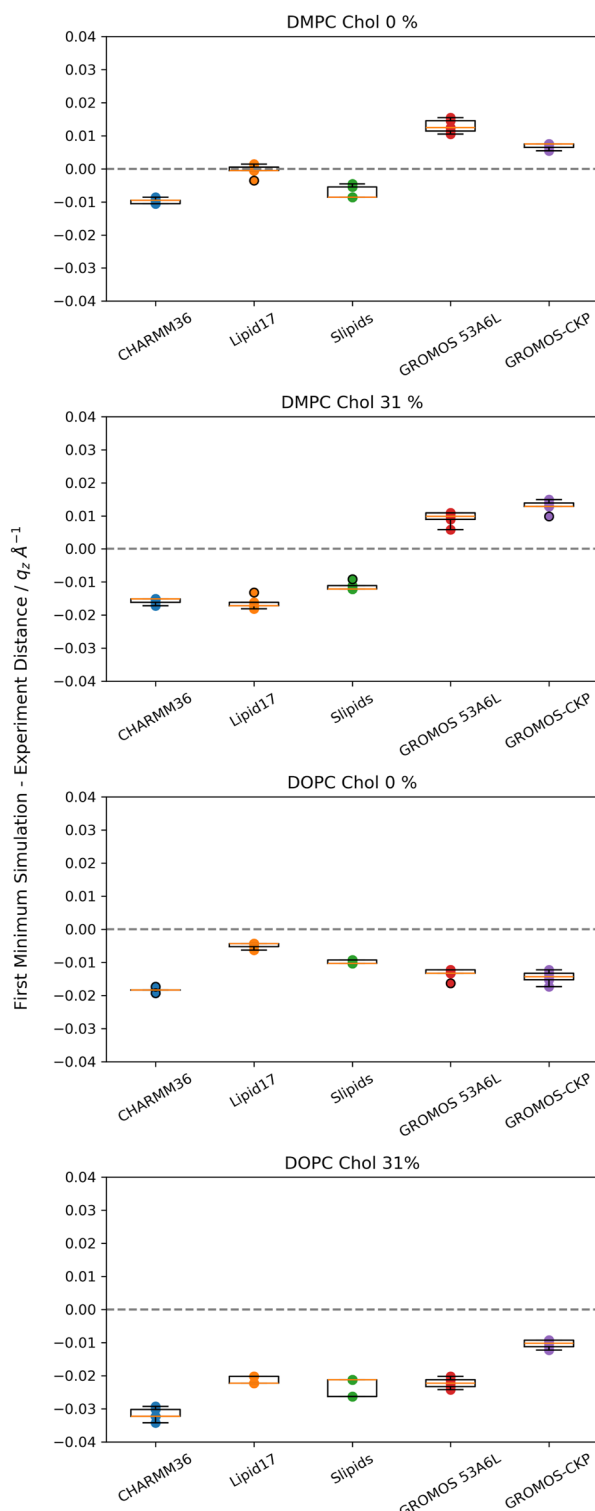


FIG. 8. Cartesian distances between the location of the first minima in x-ray form factors of experimental and simulation systems. Each data point represents an independent replica. Experimental data were recorded at 0% and 30% cholesterol mole fractions.

assignments to the resulting x-ray form factors to be reliable. Such an analysis is beyond the scope of this work.

Limited by the availability of experimental form factor data across a range of cholesterol concentrations, we compare the simulations at 0% and 30% cholesterol mole fraction to the data of Pan *et al.*¹¹ Unfortunately, the experimental data of Hung *et al.*⁷⁰ only provide x-ray intensities and not form factors. We note that the experimental data from Pan *et al.* are recorded at a cholesterol mole fraction of 30%, while the most similar simulations performed here have a cholesterol mole fraction of 31.2%. Our analysis, following that employed by the NMRlipids project,⁸¹ focuses on the location of the first minimum of the form factor plot. The precise location of the first minimum correlates with the thickness of the membrane⁸¹ and therefore will also correlate with the membrane and lipid area. The main advantage of this approach, as opposed to metrics based on residuals between the experimental and simulation data, is that the precise locations of form factor minima are invariant to the simulation box size and do not require scaling of the simulation form factors to match the relative intensity scale of experiments. While robust simulation corrections have been proposed to address the impact of system size on relative lobe heights,⁸³ these corrections were not implemented in the NMRlipids study⁸¹ and hence were not adopted here. Thus, while this method allows for a simple and more direct comparison between the simulation and experimental data, it also reduces the (already limited) amount of experimental data available for comparison.

The Cartesian distances between the experimental and simulation form factor first minimum locations are presented in Fig. 8. The experimental values taken from Ref. 11 were extracted from graphical plots using WebPlotDigitizer.⁷¹

The comparison of experimental form factor data with simulation offers a more mixed result compared to the area data. Generally, force fields more closely align with experiment for pure PC membranes compared to PC cholesterol membrane mixtures. All-atom force fields consistently under-predict the minimum location, while united-atom force fields over-predict in DMPC and under-predict in DOPC. The form factor analysis here does not show the same correlation of our previous analysis, which suggests that all-atom force fields better model cholesterol containing DMPC lipid systems. Indeed, for the lipid area analysis, CHARMM36 was one of the best performing force fields but diverges the most from experimental form factor minimum locations. This may be due to the over-reliance on only two cholesterol concentrations per lipid, compounded by using only a single point from the form factor curves. The critical lack of more experimental data is of particular concern when performing this analysis, as it necessitates excluding most of the form factor curve.

REFERENCES

- D. Casares, P. V. Escribá, and C. A. Rosselló, *Int. J. Mol. Sci.* **20**, 2167 (2019).
- K. Komatsuya, N. Kikuchi, T. Hirabayashi, and K. Kasahara, *Int. J. Mol. Sci.* **24**, 5566 (2023).
- M. Bogdanov, *Emerging Top. Life Sci.* **7**, 1 (2023).
- S. Sonnino and A. Prinetti, *Curr. Med. Chem.* **20**, 4 (2013).
- G. van Meer, D. R. Voelker, and G. W. Feigenson, *Nat. Rev. Mol. Cell Biol.* **9**, 112 (2008).
- P. Shamaprasad, C. O. Frame, T. C. Moore, A. Yang, C. R. Iacovella, J. A. Bouwstra, A. L. Bunge, and C. McCabe, *Prog. Lipid Res.* **88**, 101184 (2022).

⁷T. L. Steck and Y. Lange, *Traffic* **19**, 750 (2018).

⁸O. Edholm and J. F. Nagle, *Biophys. J.* **89**, 1827 (2005).

⁹Y. Su, Q. Li, L. Chen, and Z. Yu, *Colloids Surf., A* **293**, 123 (2007).

¹⁰M. Kodama, O. Shibata, S. Nakamura, S. Lee, and G. Sugihara, *Colloids Surf., B* **33**, 211 (2004).

¹¹J. Pan, S. Tristram-Nagle, and J. F. Nagle, *Phys. Rev. E* **80**, 021931 (2009).

¹²A. Zampelas and E. Magriplis, *Nutrients* **11**, 1645 (2019).

¹³S. L. Regen, *JACS Au* **2**, 84 (2022).

¹⁴J. B. Leathers, *Lancet* **205**, 853 (1925).

¹⁵P. Dynarowicz-Łatka and K. Hac-Wydro, *Colloids Surf., B* **37**, 21 (2004).

¹⁶M. R. Krause, M. Wang, L. Mydock-McGrane, D. F. Covey, E. Tejada, P. F. Almeida, and S. L. Regen, *Langmuir* **30**, 12114 (2014).

¹⁷M. L. Berkowitz, *Biochim. Biophys. Acta, Biomembr.* **1788**, 86 (2009).

¹⁸Y. Wang, P. Gkeka, J. E. Fuchs, K. R. Liedl, and Z. Cournia, *Biochim. Biophys. Acta, Biomembr.* **1858**, 2846 (2016).

¹⁹Q. Waheed, R. Tjörnhammar, and O. Edholm, *Biophys. J.* **103**, 2125 (2012).

²⁰S. Chiu, E. Jakobsson, R. J. Mashl, and H. L. Scott, *Biophys. J.* **83**, 1842 (2002).

²¹M. D. Daily, B. N. Olsen, P. H. Schlesinger, D. S. Ory, and N. A. Baker, *J. Chem. Theory Comput.* **10**, 2137 (2014).

²²P. Siani, H. Khandelia, M. Orsi, and L. G. Dias, *J. Comput.-Aided Mol. Des.* **32**, 1259 (2018).

²³M. Alwarawrah, J. Dai, and J. Huang, *J. Phys. Chem. B* **114**, 7516 (2010).

²⁴C. L. Armstrong, D. Marquardt, H. Dies, N. Kučerka, Z. Yamani, T. A. Harroun, J. Katsaras, A. C. Shi, and M. C. Rheinstädter, *PLoS One* **8**, e66162 (2013).

²⁵F. Leeb and L. Maibaum, *Biophys. J.* **115**, 2179 (2018).

²⁶F. De Meyer and B. Smit, *Proc. Natl. Acad. Sci. U. S. A.* **106**, 3654 (2009).

²⁷S. Wheeler, "Physical properties of mixed membranes explored using atomistic and coarse grained molecular dynamic simulations with enhanced sampling techniques," Ph.D. thesis, School of Chemistry, University of Southampton, 2018.

²⁸S. Seo and W. Shinoda, *J. Chem. Theory Comput.* **15**, 762 (2019).

²⁹A. K. Smith and D. K. Klimov, *J. Phys. Chem. B* **122**, 11311 (2018).

³⁰S. Baoukina, E. Mendez-Villuendas, W. F. Bennett, and D. P. Tieleman, *Faraday Discuss.* **161**, 63 (2012).

³¹H. Martínez-Seara, T. Ró, M. Karttunen, I. Vattulainen, and R. Reigada, *PLoS One* **5**, e11162 (2010).

³²Z. Cournia, G. M. Ullmann, and J. C. Smith, *J. Phys. Chem. B* **111**, 1786 (2007).

³³M. I. Oh, C. I. Oh, and D. F. Weaver, *J. Phys. Chem. B* **124**, 3686 (2020).

³⁴F. Fornasier, L. M. P. Souza, F. R. Souza, F. Reynaud, and A. S. Pimentel, *J. Chem. Inf. Model.* **60**, 569 (2020).

³⁵I. Ermilova and A. P. Lyubartsev, *Soft Matter* **15**, 78 (2019).

³⁶M. Javanainen, P. Heftberger, J. J. Madsen, M. S. Miettinen, G. Pabst, and O. H. S. Ollila, *J. Chem. Theory Comput.* **19**, 6342 (2023).

³⁷J. B. Klauda, R. M. Venable, J. A. Freites, J. W. O'Connor, D. J. Tobias, C. Mondragon-Ramirez, I. Vorobyov, A. D. MacKerell, and R. W. Pastor, *J. Phys. Chem. B* **114**, 7830 (2010).

³⁸F. Grote and A. P. Lyubartsev, *J. Phys. Chem. B* **124**, 8784 (2020).

³⁹I. Gould, A. Skjekv, C. Dickson, B. Madej, and R. Walker, "Lipid17: A comprehensive AMBER force field for the simulation of zwitterionic and anionic lipids" (unpublished) (2018).

⁴⁰C. J. Dickson, B. D. Madej, Å. A. Skjekv, R. M. Betz, K. Teigen, I. R. Gould, and R. C. Walker, *J. Chem. Theory Comput.* **10**, 865 (2014).

⁴¹B. D. Madej, I. R. Gould, and R. C. Walker, *J. Phys. Chem. B* **119**, 12424 (2015).

⁴²D. Poger, W. F. Van Gunsteren, and A. E. Mark, *J. Comput. Chem.* **31**, 1111 (2010).

⁴³T. J. Piggot, A. Piñeiro, and S. Khalid, *J. Chem. Theory Comput.* **8**, 4593 (2012).

⁴⁴S. J. Marrink, A. H. De Vries, T. A. Harroun, J. Katsaras, and S. R. Wassall, *J. Am. Chem. Soc.* **130**, 10 (2008).

⁴⁵M. N. Melo, H. I. Ingólfsson, and S. J. Marrink, *J. Chem. Phys.* **143**, 243152 (2015).

⁴⁶L. Borges-Araújo, A. C. Borges-Araújo, T. N. Ozturk, D. P. Ramirez-Echemendia, B. Fábián, T. S. Carpenter, S. Thallmair, J. Barnoud, H. I. Ingólfsson, G. Hummer, D. P. Tieleman, S. J. Marrink, P. C. T. Souza, and M. N. Melo, *J. Chem. Theory Comput.* **19**, 7387 (2023).

⁴⁷P. C. T. Souza, R. Alessandri, J. Barnoud, S. Thallmair, I. Faustino, F. Grünewald, I. Patmanidis, H. Abdizadeh, B. M. H. Bruininks, T. A. Wassenaar, P. C. Kroon, J. Melcr, V. Nieto, V. Corradi, H. M. Khan, J. Dománski, M. Javanainen, H. Martínez-Seara, N. Reuter, R. B. Best, I. Vattulainen, L. Monticelli, X. Periole, D. P. Tieleman, A. H. De Vries, and S. J. Marrink, *Nat. Methods* **18**, 382 (2021).

⁴⁸S. Genheden and J. W. Essex, *J. Comput.-Aided Mol. Des.* **30**, 969 (2016).

⁴⁹A. K. Malde, L. Zuo, M. Breeze, M. Stroet, D. Poger, P. C. Nair, C. Oostenbrink, and A. E. Mark, *J. Chem. Theory Comput.* **7**, 4026 (2011).

⁵⁰M. Stroet, B. Caron, M. S. Engler, J. van der Woning, A. Kauffmann, M. van Dijk, M. El-Kebir, K. M. Visscher, J. Holownia, C. Macfarlane, B. J. Bennion, S. Gelpi-Dominguez, F. C. Lightstone, T. van der Storm, D. P. Geerke, A. E. Mark, and G. W. Klau, *J. Comput.-Aided Mol. Des.* **37**, 357 (2023).

⁵¹M. Bachar, P. Brunelle, D. P. Tieleman, and A. Rauk, *J. Phys. Chem. B* **108**, 7170 (2004).

⁵²A. Kukol, *J. Chem. Theory Comput.* **5**, 615 (2009).

⁵³T. J. Piggot, I. D. Walsh, J. W. Essex, and J. R. Allison, "Testing and optimization of GROMOS force fields in GROMACS: Phospholipid membranes" (unpublished) (2024).

⁵⁴L. Martínez, R. Andrade, E. G. Birgin, and J. M. Martínez, *J. Comput. Chem.* **30**, 2157 (2009).

⁵⁵J. Nagle, R. Zhang, S. Tristram-Nagle, W. Sun, H. Petracche, and R. Suter, *Biophys. J.* **70**, 1419 (1996).

⁵⁶R. J. Mashl, H. L. Scott, S. Subramaniam, and E. Jakobsson, *Biophys. J.* **81**, 3005 (2001).

⁵⁷K. Hristova and S. H. White, *Biophys. J.* **74**, 2419 (1998).

⁵⁸M. J. Abraham, T. Murtola, R. Schulz, S. Páll, J. C. Smith, B. Hess, and E. Lindahl, *SoftwareX* **1–2**, 19 (2015).

⁵⁹A. P. Thompson, H. M. Aktulga, R. Berger, D. S. Bolintineanu, W. M. Brown, P. S. Crozier, P. J. in't Veld, A. Kohlmeyer, S. G. Moore, T. D. Nguyen, R. Shan, M. J. Stevens, J. Tranchida, C. Trott, and S. J. Plimpton, *Comput. Phys. Commun.* **271**, 108171 (2022).

⁶⁰H. J. Berendsen, J. P. Postma, W. F. Van Gunsteren, A. Dinola, and J. R. Haak, *J. Chem. Phys.* **81**, 3684 (1984).

⁶¹S. Genheden and J. W. Essex, *J. Chem. Theory Comput.* **11**, 4749 (2015).

⁶²M. Tuckerman, B. J. Berne, and G. J. Martyna, *J. Chem. Phys.* **97**, 1990 (1992).

⁶³D. J. Evans and B. L. Holian, *J. Chem. Phys.* **83**, 4069 (1985).

⁶⁴G. Bussi, D. Donadio, and M. Parrinello, *J. Chem. Phys.* **126**, 014101 (2007).

⁶⁵P.-C. Hsu, B. M. H. Bruininks, D. Jefferies, P. Cesar Telles de Souza, J. Lee, D. S. Patel, S. J. Marrink, Y. Qi, S. Khalid, and W. Im, *J. Comput. Chem.* **38**, 2354 (2017).

⁶⁶M. Parrinello and A. Rahman, *J. Appl. Phys.* **52**, 7182 (1981).

⁶⁷T. N. Heinz, W. F. van Gunsteren, and P. H. Hünenberger, *J. Chem. Phys.* **115**, 1125 (2001).

⁶⁸S. Thallmair, M. Javanainen, B. Fábián, H. Martínez-Seara, and S. J. Marrink, *J. Phys. Chem. B* **125**, 9537 (2021).

⁶⁹K. W. Vugrin, L. P. Swiler, R. M. Roberts, N. J. Stucky-Mack, and S. P. Sullivan, *Water Resour. Res.* **43**, W03423, <https://doi.org/10.1029/2005wr004804> (2007).

⁷⁰W. C. Hung, M. T. Lee, F. Y. Chen, and H. W. Huang, *Biophys. J.* **92**, 3960 (2007).

⁷¹A. Rohatgi, WebPlotDigitizer, 2024.

⁷²N. Kučerka, J. F. Nagle, J. N. Sachs, S. E. Feller, J. Pencer, A. Jackson, and J. Katsaras, *Biophys. J.* **95**, 2356 (2008).

⁷³Y. Liu and J. F. Nagle, *Phys. Rev. E* **69**, 040901(R) (2004).

⁷⁴H. M. McConnell and A. Radhakrishnan, *Biochim. Biophys. Acta, Biomembr.* **1610**, 159 (2003).

⁷⁵T. H. Chou and C. H. Chang, *Colloids Surf., B* **17**, 71 (2000).

⁷⁶T. Ró, M. Paseniewicz-Gierula, I. Vattulainen, and M. Karttunen, *Biochim. Biophys. Acta, Biomembr.* **1788**, 97 (2009).

⁷⁷T. M. Ferreira, F. Coreta-Gomes, O. H. S. Ollila, M. J. Moreno, W. L. Vaz, and D. Topgaard, *Phys. Chem. Chem. Phys.* **15**, 1976 (2013).

⁷⁸M. C. Wiener and S. H. White, *Biophys. J.* **61**, 434 (1992).

⁷⁹C. Wang, M. R. Krause, and S. L. Regen, *J. Am. Chem. Soc.* **137**, 664 (2015).
⁸⁰S. Tristram-Nagle, Y. Liu, J. Legleiter, and J. F. Nagle, *Biophys. J.* **83**, 3324 (2002).
⁸¹A. M. Kiirikki, H. S. Antila, L. S. Bort, P. Buslaev, F. Favela-Rosales, T. M. Ferreira, P. F. J. Fuchs, R. Garcia-Fandino, I. Gushchin, B. Kav, N. Kučerka, P. Kula, M. Kurki, A. Kuzmin, A. Lalitha, F. Lolicato, J. J. Madsen, M. S. Miettinen, C.

Mingham, L. Monticelli, R. Nencini, A. M. Nesterenko, T. J. Piggot, Á. Piñeiro, N. Reuter, S. Samantray, F. Suárez-Lestón, R. Talandashti, and O. H. S. Ollila, *Nat. Commun.* **15**, 1136 (2024).

⁸²N. Kučerka, J. Katsaras, and J. F. Nagle, *J. Membr. Biol.* **235**, 43 (2010).

⁸³A. R. Braun, E. G. Brandt, O. Edholm, J. F. Nagle, and J. N. Sachs, *Biophys. J.* **100**, 2112 (2011).